Study of hydrotreating performances of trimetallic NiMoW/Al_2O_3 catalysts prepared from mixed MoW Keggin heteropolyanions with various Mo/W ratios

A. Kokliukhin[a,b], M. Nikulshina[a], A. Mozhaev[a,c,e], C. Lancelot[b], P. Blanchard[b], V. Briois[d], M. Marinova[f], C. Lamonier[b*], and P. Nikulshin[a,c,e]**

[a] *Samara State Technical University, 244, Molodogvardeyskaya st., Samara, 443100, Russia*

[b] *Univ. Lille, CNRS, Centrale Lille, ENSCL, Univ. Artois, UMR 8181 – UCCS – Unité de Catalyse et Chimie du Solide, F-59000 Lille, France*

[c] *All-Russia Research Institute of Oil Refining, 6/1 Aviamotornaya st., Moscow, 111116, Russia*

[d] *Synchrotron SOLEIL, CNRS-UR1, BP 34, L'Orme des Merisiers, Gif-sur-Yvette, France*

[e] *Gubkin Russian State University of Oil and Gas, Leninskiy Prospect 65, Moscow, 119991, Russia*

[f] *Univ. Lille, CNRS, INRA, Centrale Lille, ENSCL, Univ. Artois, FR 2638 - IMEC - Institut Michel-Eugène Chevreul, F-59000 Lille*

[*] Corresponding author at: Université Lille, UMR 8181 CNRS, UCCS, Villeneuve d'Ascq, France.

[**] Corresponding author at: Samara State Technical University, 244 Molodogvardeyskaya st., Samara 443100, Russia.

E-mail: p.a.nikulshin@gmail.com (Pavel Nikulshin), carole.lamonier@univ-lille.fr (Carole Lamonier).

Abstract

Trimetallic NiMoW/Al_2O_3 catalysts based on mixed $H_4[SiMo_nW_{n-12}O_{40}]$ (n = 1, 3, 6 and 9) Keggin-type heteropolyacids (HPAs) were synthesized by incipient wetness impregnation of alumina with aqueous solutions of mixed HPAs. For comparison purposes, trimetallic samples were prepared from a mixture of monometallic $H_4[SiMo_{12}O_{40}]$ and $H_4[SiW_{12}O_{40}]$ HPAs with a Mo/W ratio corresponding to the mixed MoW HPAs. The catalysts were sulfided by liquid phase method and tested in the model reactions of

dibenzothiophene hydrodesulfurization (DBT HDS) and naphthalene hydrogenation (HYD), with subsequent addition of quinoline to study the effect of inhibition of target reactions. Further, the catalysts were tested in the hydrotreating of straight-run gas oil (SRGO) to evaluate the efficiency of catalysts on real feedstocks. In order to link catalytic performances with the preparation method and Mo/W ratio, the catalysts were fully characterized by high-resolution transmission electron microscopy (HRTEM), X-ray photoelectron spectroscopy (XPS), high angle annular dark field imaging (HAADF) and Quick X-ray absorption spectroscopy (XAS). It was found that Mo/W atomic ratio of the structure-forming metals in the active phase, deriving from the Mo/W ratio in the HPA precursor, directly affects the ratio of the hydrogenation and hydrodesulfurization performances. For feedstock with a high concentration of N-containing compounds, it is necessary to use mixed NiMoW systems with a high tungsten percentage in order to reduce the inhibitory effect and ensure the quality of the products. The use of new mixed MoW Keggin HPAs has made it possible to enhance the synergistic effect in trimetallic NiMoW catalysts due to the closer interaction between Mo and W, which increased the sulfidation degree of metals and also contributed to the formation of highly active mixed NiMoWS sites.

Keywords: Hydrodesulfurization, hydrogenation, hydrodenitrogenation, NiMoW mixed phase, straight run gas oil, EXAFS.

1. Introduction

Deteriorating quality of processed raw materials and stiffening of environmental standards to motor fuels create significant difficulties for oil refining. The latest Euro-6 environmental standard for gasoline and diesel fuel was introduced in 2015 [1] with the main objective to reduce the emission of harmful substances, and primarily to reduce the emission of nitrogen oxides (NO_x) and residual hydrocarbons (HC). To face these new regulations, most refiners have started new developments to improve their hydrotreating and hydrocracking processes to meet the required nitrogen removal standards and saturation of aromatics. Therefore, trimetallic catalytic systems, able to provide the

required level of hydrodenitrogenation (HDN), together with a resistance to the inhibition effect of nitrogen-containing compounds, are now being actively investigated [2-6]. These trimetallic catalytic systems can be conditionally divided into two large groups, according to the type of preparation: i) co-promotion, when there are two promoting metals in the structure of the active phase (for example, Co and Ni) [7,8] and ii) co-structuring, when two structure-forming metals of the active phase (Mo and W) are present in the system [9-13].

Many studies of the co-promotion effect showed that the NiCoMo systems could have higher activities in hydrotreating reactions due to the optimization of the electron density on the anti-bonding *d*-orbital of Mo in the active phase. It was also found that the maximum effect is achieved when CoMo systems are promoted by Ni, while the promoting effect of Ni to Mo/Al_2O_3 almost disappears with the addition of cobalt to $Ni\text{-}Mo/Al_2O_3$ catalysts, which suggests that Co prevents the formation of the high active NiMoS phase [14]. Recently, Mashayekhi et al. [15] performed a study of NiCoMo alumina-supported catalyst. The absence of synergistic effect of co-promotion observed can be explained by the fact that promoters were simultaneously introduced into the structure. In this case, Co reacts faster with supported MoS_2 than Ni, whatever the support, thereby forming only a monopromoted system, while Ni transforms to massive nickel sulfides and blocks access to CoMoS edge sites [16]. In contrast, Medina Cervantes et al. [17] reported a slight increase of activity in HDS of DBT of $CoNi_{0.05}Mo/Al_2O_3$ catalyst prepared by co-impregnation method compared to $CoMo/Al_2O_3$. The use of citric acid as a chelating agent has been reported for facilitating the incorporation of Ni atoms into the structure of the active phase [18-20] and it was shown that simultaneous use of $NiCO_3$, citric acid and Co_2Mo_{10}HPA improves the co-promotion effect due to the proximity of cobalt, nickel and molybdenum atoms in the starting materials [7].

Much attention has been given to the promoted MoW catalytic system. The comparison of the promoting effect in trimetallic CoMoW and NiMoW systems was reported [21]. It was found that a synergistic effect from the use of trimetallic catalysts is observed only when MoW/Al_2O_3 is promoted by Ni, while in Co-promoted samples the activity only depends on the molybdenum content. These

results were consistent with those obtained by Thomazeau et al [22]. Indeed, using the density functional theory (DFT) calculations based on linear interpolation model of surface ΔE_{MS} between the binary NiMoS and NiWS, these authors found a synergistic effect only in mixed NiMoW catalysts. This effect was also confirmed by catalytic tests in thiophene HDS and hydrotreating of SRGO, while no synergistic effect was noticed in the promoted by Co atoms and unpromoted systems.

Currently, the researchers cannot fully explain the nature of the high activity of NiMoW mixed sulfides. However, studies are underway to consider such important aspects as the influence of the type of promoter [21, 23], promotion degree [24], sulfidation procedure [11, 25] and the Mo/W ratio [12-13] on the structure of the active phase and catalytic activity.

Hein et al. [26], using X-ray absorption spectroscopy and STEM-HAADF, showed that mixed $Mo_{1-x}W_xS_2$ intralayer particles of bulk NiMoW trimetallic catalysts lead to higher concentrations of edge-incorporated Ni compared to bimetallic (NiMo and NiW) analogues. Van Haandel et al. [11] found that the structure of the mixed NiMoW active phase may differ, depending on the sulfidation conditions. Authors established the formation of two different structures in a different arrangement of Mo and W atoms: i) “core-shell” structure (Mo atoms are surrounded by W atoms); ii) “random” structure (Mo and W atoms are disordered in the crystallite). These core-shell and random structures were also evidenced in unpromoted MoW/Al_2O_3 catalysts based on mixed Keggin-type $SiMo_nW_{12-n}$HPAs. It was shown that the structure of the mixed active phase depends on the type of sulfidation (liquid or gas phase) [25]. Gas phase activation led to the formation of more efficient $MoWS_2$ particles with “core-shell” structure, these catalysts were more efficient than those activated by liquid phase sulfidation where Mo was randomly distributed inside the WS_2 slabs [13]. Recently Mashayekhi et al. [15] performed a study of NiMoW alumina-supported catalyst with different Mo/W ratios. It was found that the co-structuring catalyst with the lowest Mo/(Mo +W) atomic ratio had the highest activity in SRGO hydrotreating

The synthesis technique and the method of introducing metals into a catalyst play an important role. Traditionally, ammonium heptamolybdate (AHM), ammonium paratungstate, ammonium metatungstate (AMT) and ammonium tungstate are used as precursors for the synthesis of mixed

(Ni)MoW catalysts [23, 27, 28]. Studies have shown that the use of mixed MoW Keggin HPAs precursors for the preparation of unpromoted MoW catalysts enhances the effect of co-structuring to form mixed $MoWS_2$ phase due to the closer interaction of both structure-forming metals (Mo and W) during sulfidation. The formation of high amount of mixed active phase species was confirmed by XAS, HAADF and ToF-SIMS analysis [13, 25, 29].

Nevertheless, this effect of mixed active phase formation may differ for promoted $MoWS_2$ catalytic systems. Thomazeau et al. noted that for unpromoted catalysts, prepared from a mixture of AHM and AMT, this synergistic effect was not detected and the activity in thiophene HDS of the catalysts increased linearly with an increase of molybdenum percentage in the samples [22]. The introduction of nickel into the catalyst composition had a positive effect on mixed systems. This effect has not yet been studied for catalysts prepared from mixed MoW-heteropolyanion precursors of active phase.

Therefore, the aim of this work was to study hydrotreating performances of trimetallic $NiMoW/Al_2O_3$ catalysts prepared from a mixed bimetallic $SiMo_nW_{12-n}$HPAs (where n = 1, 3, 6 and 9) in comparison with samples synthesized from a mixture of two monometallic $SiMo_{12}$ and SiW_{12}HPAs. The catalysts were studied in co-hydrotreating of dibenzothiophene and naphthalene with the addition of a nitrogen-containing inhibitor, as well as in hydrotreating of a SRGO. For a better understanding of the promoter effect on the composition and structure of the active phase, the samples were analyzed by HRTEM and XPS. In order to evaluate more specifically the effect of the addition of a promoter and the formation of the mixed MoWS slabs, selected trimetallic catalysts were analyzed by Quick XAS and STEM-HAADF imaging.

2. Experimental

2.1 Synthesis of NiMo(W)/Al_2O_3 catalysts

Catalysts with fixed surface density of the metals *d*(Mo+W) equal to 4 at nm^{-2} and Ni/(Mo+W) ratio = 0.5 were synthesized by simultaneous impregnation of alumina [γ-Al_2O_3 (Norton), specific area:

240 m^2 g^{-1}, pore volume: 0.9 mL g^{-1}] *via* the wetness impregnation method using aqueous solution of HPAs, citric acid (CA) and nickel carbonate (CA/Ni molar ratio was equal to 1:1). The mixed $H_4[SiMo_nW_{12-n}O_{40}]$ HPAs with different Mo/W atomic ratio have been synthesized according to previous reports [13]. Four trimetallic catalysts were prepared using mixed HPAs (hereafter $NiMo_nW_{12-n}/Al_2O_3$). Moreover, trimetallic samples with a Mo/W ratio corresponding to the composition of the mixed $SiMo_nW_{12-n}$ HPAs were synthesized using a mixture of monometallic Mo and W HPAs, and will be denoted $Ni(Mo_n+W_{12-n})/Al_2O_3$. The bimetallic catalysts based on monometallic $H_4[SiMo_{12}O_{40}]$ and $H_4[SiW_{12}O_{40}]$ HPAs were prepared for comparison and denoted as $NiMo_{12}/Al_2O_3$ and NiW_{12}/Al_2O_3, respectively. The synthesis was carried out as follows: CA was dissolved in distilled water, then the solution was heated to 60-70°C and nickel carbonate was added slowly under stirring (for better dissolution). The solution was stirred until complete dissolution under a watch glass (~40 min), then cooled to 35-40°C. The corresponding HPA was added under stirring to the nickel citrate complex, and then the support was impregnated by the resulting solution. After maturation (in a desiccator with high wetness at room temperature for 2 h), the oxidic catalysts were dried at 60°C (4 h), 80°C (2 h) and 100°C (4 h) in air atmosphere without further calcination. The metal compositions in the solids were obtained using an EDX800HS Shimadzu X-ray fluorescence analyzer and are given in **Table 1**. For further investigation, all catalysts were sulfided at 3.0 MPa of hydrogen, 2 h^{-1} LHSV and a 300 NL L^{-1} volume ratio of hydrogen to feed by a mixture of dimethyl disulfide (DMDS) with 6 wt. % of sulfur in toluene at 240°C for 10 h and at 340°C for 8 h. For characterization of the active phase, sulfided catalysts were unloaded from the reactor for analysis in a glove box in an inert gas atmosphere (argon). The samples were transferred to glass vials with n-heptane to avoid reoxidation. The absence of any signal at 169.0 eV in the S2p XPS spectra (characteristic of sulfates) indicates that sulfided catalysts were not reoxidized during their transfer from the sulfiding reactor to the XPS instrument.

2.2 Textural characteristics of the catalysts

The textural properties of sulfided catalysts were measured using the Quantachrome Autosorb-1. Before being measured, the samples were outgassed under vacuum (< 10^{-1} Pa) at 300°C for 3 h. The

specific surface area (SSA) was calculated using the Brunauer-Emmett-Teller method at relative partial pressures (P/P_0) ranging from 0.05 to 0.3. Total pore volume (at P/P_0 of 0.99) and pore size distribution were obtained using the desorption curve and the Barret-Joyner-Halenda model.

2.3 High-resolution transmission electron microscopy (HR-TEM)

The morphology of $Mo(W)S_2$ nano-crystallites in $NiMo(W)/Al_2O_3$ samples was investigated by HR-TEM using a Tecnai G2 20 electron microscope with LaB_6 filament with a 0.19 nm lattice-fringe resolution and an accelerating voltage of 200 kV. The suspension of samples was deposited on carbon films supported on copper grids. In the high-resolution mode, 20-30 micrographs were obtained for each catalyst. The length and stacking of at least 500 slabs were measured using ImageJ free software. Assuming that the $NiMo(W)S_2$ slabs were perfect hexagons [30], dispersion (D) of $Mo(W)S_2$ phase was statistically evaluated by dividing the total number of Mo(W) atoms at the edge of average crystallite of $Mo(W)S_2$ (W_e), plus corner Mo(W) atoms (W_c), by the total number of Mo(W) atoms (W_T) using the slab sizes measured in the TEM micrographs [31]:

$$D = \frac{W_e + W_c}{W_T} = \frac{\sum_{i=1..t} 6n_i - 6}{\sum_{i=1..t} 3n_i^2 - 3n_i + 1}, \quad (1)$$

where n_i is the number of Mo(W) atoms along one side of the $Mo(W)S_2$ slab, as determined by its length, and t is the total number of slabs in the TEM micrograph.

The number of slabs per stack was determined to obtain the average stacking degree ($\overline{N}$):

$$\overline{N} = \frac{\sum_{i=1..t} n_i N_i}{\sum_{i=1..t} n}, \quad (2)$$

where n_i is the number of stacks in N_i layers.

2.4 X-ray photoelectron spectroscopy (XPS)

XPS spectra of sulfided catalysts were recorded on a Kratos Axis Ultra DLD spectrometer using a monochromatic Al Kα source (hν = 1486.6 eV, 150 W). The samples were mounted on a holder using

double-sided adhesive tape. The recharging effect, arising from the photoemission of electrons, was minimized by irradiating the sample surface with slow electrons from a special source (flood gun). Binding energy (BE) values were ascribed to the positions of the Au $4f_{7/2}$ peak at 83.96 eV and Cu $2p_{3/2}$ peak at 932.62 eV. Narrow spectral regions (Al 2p, S 2p, Mo 3d, W 4f, C 1s, O 1s, Ni 2p) were recorded and analyzed using the CasaXPS software program (Version 2.3.16) according to [20, 32]. Spectra were charge-corrected to provide the C 1s spectral component of adventitious carbon (C–C, C–H) at 284.8 eV. Shirley background subtraction and Gaussian (30%) Lorentzian (70%) peaks were used to decompose the spectra.

2.5 High resolution High-Angle Annular Dark-Field (HR-HAADF)

High resolution high-angle annular dark-field (HR-HAADF) imaging has been performed at 200 kV on a TITAN Themis FEI scanning transmission electron microscope (STEM). The microscope is equipped with a monochromator and a Cs probe corrector. For HAADF acquisition, the spot size was 9 with a screen current of ~50 pA, semi-convergence angle of 21 mrad and camera length of 115 mm, corresponding to collection angles for the HAADF detector between ~50 and ~200 mrad. More than 50 images were observed on each studied catalyst.

Prior to the HAADF analysis, the catalysts were sulfided in gas phase. The sulfidation was performed in a flow of 10 % H_2S in H_2 at atmospheric pressure with heating from room temperature to 400 °C with a heating rate of 3 °C/min followed by a plateau of 2 h.

2.6 Quick X-ray absorption spectroscopy (XAS)

Quick XAS was employed to follow *in situ* sulfidation of Mo, W and Ni in alumina supported trimetallic hydrotreating catalysts. XAS measurements were carried out at the ROCK beamline at the SOLEIL synchrotron [33]. Oxide catalysts were ground and loaded in the cell [34], where they were gas-phase sulfided in the same way as for HR-HAADF analysis. Spectra were recorded in transmission mode. The use of the remotely-controlled edge jumping capability of the beamline allows to record XAS spectra alternately at the Ni and Mo *K*-edges and W L_1-, L_2-, L_3-edges on the same sample during one

sulfidation procedure [33]. At the end of sulfidation, the cell was cooled down at room temperature and 1180 spectra at each edge for the as-sulfided catalysts were recorded and merged. Extended X-ray absorption fine structure (EXAFS) spectra were background-subtracted with Athena and fitted with Artemis, which is an interface to IFEFFIT [35].

The following structural parameters were determined during the fit: interatomic distances (R), coordination numbers (N), Debye-Waller factors (σ^2) and energy shifts (ΔE_0). To reduce the number of variables, Debye-Waller factor for Mo−Mo, W−W and Mo-W paths were set equal. Furthermore, taking into account the size of sulfide particles, no Mo−Ni or W−Ni path has been used for the fitting because this contribution, if it exists, is in insignificant proportion at the Mo K- or W L_3-edges. The Fourier transforms (FT) of the measured spectra were modeled with a k-weight of 1, 2, and 3. Amplitude reduction factors (S_0^2) were obtained by fitting bulk MoS_2 and WS_2 references. The fit range of Mo K-edge spectra was Δk = 3-14 $Å^{-1}$ and ΔR = 1.4-3.4 Å and the range of W L_3-edge spectra was Δk = 4.1-14.5 $Å^{-1}$ and ΔR = 1.4-3.43 Å.

2.7 Evaluation of catalytic activities

2.7.1 Evaluation of catalytic activity in hydrotreating of model feedstock

A series of catalytic tests was carried out in the process of co-hydrotreating of dibenzothiophene (DBT) (1000 ppm S) and naphthalene (3 wt. %) with the addition of a nitrogen-containing component (quinoline, 500 ppm N) in order to determine the inhibition effect on trimetallic NiMoW/Al_2O_3 catalysts. A mixture of 0.2 g of catalyst (0.25 – 0.50 mm) and low-surface-area sieved carborundum (0.2–0.4 mm) in a ratio of 1:1 was loaded into the isothermal zone of fixed-bed microreactor. Prior to the catalytic activity tests, the catalysts were sulfided by a mixture of DMDS (6 wt.% of sulfur) in toluene sequentially at 240°C for 10 h and at 340°C for 8 h, 3.0 MPa of hydrogen. Catalysts were tested under 280°C, 3.0 MPa of hydrogen, 40 h^{-1} liquid hourly space velocity (LHSV) and a 500 NL L^{-1} volume ratio of hydrogen to feed. Several samples were tested twice to confirm the results. For these samples, average values of catalytic activity are presented. The liquid product compositions were identified by GC/MS analysis and

determined every hour using a Crystall-5000 GC equipped with a 30 m OV-101 column. Helium was used as the carrier gas. The temperature of injector and flame ionization detector were 240 and 250 °C, respectively. The column was temperature programmed from 140 °C (4 min) at a rate of 6 °C/min to 150 °C (1 min) and to 240 °C at a rate of 10 °C/min. All catalysts exhibited stable performance, achieving a steady state after 7 – 10 h. According to many studies, the kinetics of the HDS, HDN and HYD reactions for a plug-flow reactor are described by the Langmuir-Hinshelwood model, taking the interaction between the adsorbed organic molecule and the adsorbed hydrogen as the limiting stage (see supporting information). The rate constants of the DBT HDS, naphthalene HYD and quinoline HDN can be determined using the pseudo-first order kinetic equations [7, 20, 36]:

$$k_{HDS} = -\frac{F_{DBT}}{W} ln(1 - x_{DBT}),\ k_{HYD} = -\frac{F_{Naph}}{W} ln(1 - x_{Naph}),\ k_{HDN} = -\frac{F_{Qui}}{W} ln(1 - x_{HDN}) \quad (3)$$

where k is the reaction rate constants (mol g^{-1} h^{-1}), x_{DBT} and x_{Naph} are the conversions (%) of DBT and naphthalene, F is the reactant flows in moles (mol h^{-1}) and W is the weight of the catalyst (g). The degree of nitrogen removal x_{HDN} was calculated as the fraction of nitrogen removed from the initial amount of quinoline:

$$x_{HDN} = \frac{C_H}{C_N + C_{Qui} + CC_H} \times 100\% \quad (4)$$

where x_{HDN} is the nitrogen removal degree (%); C_H is the concentration (mol. %) of HDN products not containing nitrogen (propylbenzene, propylcyclohexane); C_N is the concentration (mol.%) of HDN products containing nitrogen (tetrahydroquinoline, o-aminopropylbenzene, o-aminopropylcyclohexane); C_{Qui} is the concentration (mol. %) of quinoline after reaction.

Since quinoline rapidly turns into tetrahydroquinoline, simple conversion of quinoline does not allow us to compare the samples correctly as well as to evaluate HDN activity. The same approach to estimate the conversion of nitrogen-containing compounds was used in [7, 37]. In eq. 4, the sum in the denominator corresponds to the sum of all the products and quinoline itself and represents the material balance for the reaction.

The HDS products from DBT included biphenyl (BP) via the direct desulfurization (DDS) pathway, as well as cyclohexylbenzene (CHB) and dicyclohexyl (DCH) from the HYD pathway. Only traces of hydrogenated tetrahydro- and hexahydrodibenzothiophenes were observed. The HYD/DDS selectivity was calculated according to the reaction network for DBT HDS:

$$S_{HYD/DDS} = \frac{k_{HYD}}{k_{DDS}} = \frac{C_{CHB}+C_{DCH}}{C_{BP}} \quad (5)$$

where C_{CHB}, C_{BCH} and C_{BP} are the concentration (mol. %) of CHB, DCH and BP in the reaction products, respectively.

The inhibiting factor for the DBT HDS and naphthalene HYD reaction in the presence of quinoline was calculated using the following equations:

$$\theta_{HDS} = \frac{k^0_{HDS}-k_{HDS}}{k^0_{HDS}} \times 100\% \text{ and } \theta_{HYD} = \frac{k^0_{HYD}-k_{HYD}}{k^0_{HYD}} \times 100\% \quad (6)$$

where k^0 is the rate constant (mol $g^{-1}h^{-1}$) in absence of quinoline; k is the rate constant with the addition of quinoline in feedstock (mol $g^{-1}h^{-1}$).

The turnover frequencies (*TOF*, s^{-1}) normalised on edge sites of $NiMo_nW_{12-n}S_2$ slabs for the HDS of DBT, HYD of naphthalene and HDN of quinoline allowed to a better understanding of the catalytic properties of the active phase species. *TOF* values were calculated using the following equations [29]:

$$TOF_{\text{edge}} = \frac{F \cdot x}{W \cdot \left(\frac{C_{WS_2}}{Ar_W}+\frac{C_{MoS_2}}{Ar_{Mo}}\right) \cdot D \cdot 3600} \quad (7)$$

where F is the reactant flow (mol h^{-1}); x is the conversion (%) of reactants; W is the weight of the catalyst (g); C_{WS_2} and C_{MoS_2} are the effective content of W and Mo in WS_2 and MoS_2 states, respectively (wt. %); D is the dispersion of $NiMo_nW_{12-n}S_2$ species; Ar_W and Ar_{Mo} are the standard atomic weight of tungsten (183.9 g/mol) and molybdenum (95.9 g/mol), respectively.

2.7.2 Evaluation of catalytic activity in hydrotreating of SRGO

Samples of NiMo(W) catalysts (10 g) with a particle size of 1-3 mm (bulk density equal to 0.9±0.02 cm^3g^{-1}) and low-surface-area sieved carborundum (0.2–0.4 mm) were loaded into a steel

reactor bed at a ratio of 1:2. This loading system with inert material was used to ensure uniform distribution of the feedstock over the catalyst bed. The tests were carried out at 340°C, 4.0 MPa of hydrogen, 2 h^{-1} LHSV and a 700 NL L^{-1} volume ratio of hydrogen to feed. Before testing, the catalysts had been sulfided according to the procedure described above. SRGO of West Siberian oil with boiling range 180-360°C was used as feedstock with a density at 20°C of 0.841 kg/m^3, the sulfur and nitrogen contents are 0.815 wt. % and 156 ppm, respectively. The content of sulfur and nitrogen in the feedstock and hydrogenated product was determined by elemental analysis on a Multi EA 5000 analyzer (analysis error ± 0.1 ppm), Analytik Jena. The content of mono-, bi- and polycyclic aromatic hydrocarbons was determined by HPLC on an LC-20 Prominence chromatograph, Shimadzu. All catalysts showed steady state activity after 24 h of continuous testing. Some samples were tested twice under straight run gas oil hydrotreating conditions to confirm the results.

The polycyclic aromatic hydrocarbons (PAH) hydrogenation and hydrodenitrogenation degrees over the catalysts were calculated according to the equations: $HYD = \frac{C^0_{PAH} - C_{PAH}}{C^0_{PAH}} \times 100\%$, and $HDN = \frac{N_0 - N}{N_0} \times 100\%$ (8)

where C^0_{PAH} and N_0 are PAH and nitrogen content in the feedstock, respectively; C_{PAH} and N are PAH and nitrogen content in the hydrogenation products, respectively.

The apparent HDS reaction order for middle distillates was calculated based on experimental results from [38,39] according to the following equation:

$$n = 0.2156 S_0 + 1.2823 \quad (9)$$

The apparent reaction order in the present work was equal to ~1.4 which is typical for a straight-run gas-oils and consistent with the literature data [38,40,41].

Apparent HDS rate constant was calculated as follows [39]:

$$k_{HDS} = \frac{LHSV}{n-1}\left[\frac{1}{S^{n-1}} - \frac{1}{S_0^{n-1}}\right] \times 100\% \quad (10)$$

where *LHSV* is the feed hourly space velocity (h^{-1}); *n* is the apparent reaction order; S^{n-1} and S_0^{n-1} are the concentrations of sulfur in the hydrogenation product and in the initial feedstock (wt. % of sulfur), respectively.

3. Catalytic results

3.1 NiMo(W)/Al_2O_3 catalysts in hydrotreating of DBT and naphthalene

Results of the catalytic activities of the sulfided NiMo(W)/Al_2O_3 catalysts in hydrotreating of DBT and naphthalene are presented in **Table 2**. DBT HDS and naphthalene HYD conversions varied in a wide range, from 42.0 to 73.2% and from 32.1 to 49.2 %, respectively. **Fig. 1a** shows that HDS activity noticeably increases with an increase in the proportion of molybdenum in the catalyst composition. All trimetallic $NiMo_nW_{12-n}/Al_2O_3$ catalysts based on mixed HPAs are more active than their $Ni(Mo_n+W_{12-n})/Al_2O_3$ counterparts and even surpass the $NiMo_{12}/Al_2O_3$ sample in HDS activity. The maximum of HDS activity is achieved at a Mo/(Mo+W) atomic ratio of 0.75, regardless of the type of precursor. It should be noted that HDS activity of the catalysts obtained from mixed HPAs are more impacted by molybdenum concentration, which may be due to the difference in nature of the active phase formed.

In order to estimate the effect of the use of trimetallic systems against bimetallic ones for catalytic activity, the HDS rate constant values for all NiMoW catalysts were calculated by additive way using the data for $NiMo_{12}/Al_2O_3$ and NiW_{12}/Al_2O_3 samples. Trimetallic catalysts prepared by using mixed MoW HPAs had at least 1.3 times higher values of rate constant in HDS of DBT than predicted ones, which supports the proposal about the formation of mixed NiMoWS sites developing more active sites for HDS. On the contrary, only $Ni(Mo_9+W_3)/Al_2O_3$ demonstrated surpassed activity, while the other references had lower activity than that was predicted and shown as dotted line (**Fig. 1a**).

The HDS DBT reaction mainly proceeds along the preliminary hydrogenation route. **Fig. 1c** shows that the introduction of one molybdenum atom in the $Ni(Mo_1+W_{11})/Al_2O_3$ catalysts contributes to a sharp shift in the reaction to the route of pre-hydrogenation. Further, with an increase of the Mo/(Mo+W) atomic ratio from 0.08 to 0.50, a gradual decrease in $S_{HYD/DDS}$ selectivity occurs. However, in case of $NiMo_9W_3/Al_2O_3$ catalyst, there is a slight increase in selectivity. For $Ni(Mo_n+W_{12-n})/Al_2O_3$ catalysts, the

selectivity decreases from 0.51 to 0.20 linearly with an increase in molybdenum content. The $NiMo_{12}/Al_2O_3$ catalyst exhibits the lowest $S_{HYD/DDS}$ selectivity.

At the same time, bimetallic $NiMo_{12}/Al_2O_3$ sample was the most active in naphthalene HYD reactions (**Fig. 1b**). The conversion of naphthalene HYD almost does not change with an increase in the Mo/(Mo+W) atomic ratio in the catalysts based on mixed HPAs and varies in the range of 37-39 %, while for $Ni(Mo_n+W_{12-n})/Al_2O_3$ catalysts the activity passes through a minimum at a ratio of 0.50. As in the DBT HDS, mixed $NiMo_nW_{12-n}/Al_2O_3$ catalysts are superior to reference samples prepared from a mixture of monometallic HPAs in HYD of naphthalene, as evidenced by the calculated reaction rate constants (**Table 2**).

The activity of edge centers, depending on the composition and characteristics of the active phase, was assessed by the turnover frequencies (TOF_{edge}). The *TOF* values varied from 2.99 to 4.25 $\times 10^3$ s^{-1} for DBT HDS and from 7.9 to 14.5 $\times 10^3$ s^{-1} for naphthalene HYD (**Table 2**). The maximum performance for naphthalene HYD of the edge centers corresponds to the NiW_{12}/Al_2O_3 catalyst. It should be noted that the introduction of molybdenum into the catalyst reduces the *TOF* numbers for $NiMo_nW_{12-n}/Al_2O_3$ in naphthalene HYD. At same time, in the case of DBT HDS, the differences between both types of catalysts are insignificant and no definite pattern can be traced.

3.2 NiMo(W)/Al_2O_3 catalysts in co-hydrotreating of DBT, naphthalene and quinoline

The catalytic properties of the sulfided $NiMo(W)/Al_2O_3$ catalysts in co-hydrotreating of DBT, naphthalene and quinoline are given in **Table 3**. The DBT and naphthalene conversion during the tests varied from 60.0 to 79.6 % and from 4.0 to 14.2%, respectively. A detailed analysis of the reaction products showed that diphenyl was the main reaction product, which means that the direct desulfurization is the preferred reaction route, as evidenced by the selectivity values (**Table 3**). The presence of only traces of tetrahydro-, perhydrodibenzothiophenes, as well as cyclohexylbenzene and bicyclohexyl, is due to the strong inhibitory effect of quinoline on the hydrogenation function. In the case of HYD of naphthalene, only tetralin was found in the reaction products.

More than 99% of quinoline was converted to tetrahydroquinoline under hydrotreating conditions, while the degree of nitrogen removal was only 10.2–21.2%. The maximum activity in all model reactions was observed for the $NiMo_1W_{11}/Al_2O_3$ sample (**Fig. 2**), as evidenced by the calculated reaction rate constants. Further increase in the proportion of Mo in the composition of the catalyst leads to a decrease in the catalytic activity in all studied reactions. Moreover, the greatest drop in activity for mixed $Ni(Mo_nW_{12-n})/Al_2O_3$ is observed when the Mo/(Mo+W) ratio goes from 0.08 to 0.25 **(Fig. 2)**. It should be noted that when quinoline was added to the feed, only $NiMo_1W_{11}/Al_2O_3$ sample significantly exceeded the additive values (**Fig. 2a**).

The introduction of quinoline into the model mixture promoted a slight increase in HDS activity, as evidenced by the obtained values of the inhibition effect (**Fig. 3a**). This effect is pronounced for bimetallic and trimetallic catalysts with high W percentages in the catalysts. It should be noted that this effect weakens with an increase in the Mo/(Mo+W) atomic ratio and turns into inhibition on both types of catalysts. The highest inhibiting effect for DBT HDS is manifested for catalysts based on mixed $SiMo_nW_{12-n}$HPAs with Mo/(Mo+W) atomic ratio more than 0.25, but at the same time the $NiMo_nW_{12-n}/Al_2O_3$ catalysts provide a higher DBT conversion. $NiMo_1W_{11}/Al_2O_3$ sample was less sensitive to quinoline, which is typical for NiW_{12}/Al_2O_3 catalyst, but the activity of the bimetallic sample was lower.

The inhibition of the reaction by the N-containing component is more intense for naphthalene HYD, which is consistent with literature data [42]. The inhibitory effect of naphthalene HYD ranges from 67 to 91 % **(Fig. 3b)**. The $NiMo_{12}/Al_2O_3$ bimetallic catalyst was the most affected by quinoline inhibition effect. Naphthalene HYD performance of catalysts prepared from a mixture of monometallic HPAs are a little bit more affected by quinoline than the samples prepared from the mixture of monometallic HPAs. As in the case of the HDS reaction, the inhibition degree in the naphthalene HYD depends on the atomic ratio of the structure-forming metals of the active phase. It should be noted that the increase in the atomic ratio more than 0.25 almost does not change the degree of inhibition, which varies only around 1-2%.

The calculated TOF_{edge} numbers, after adding quinoline to the model feed, are shown in **Table 3**. The addition of quinoline leads to a decrease in the efficiency of edge active centers in both the DBT HDS and naphthalene HYD reaction. It should be noted that the addition of quinoline creates certain patterns for both types of catalysts, which was not observed in the previous section. An increase in molybdenum content in trimetallic catalysts decreases the activity of the edge centers in both reactions. As noted earlier, an increase in the Mo/(Mo+W) ratio more than 0.08 leads to the equalization of the *TOF* values, regardless of the type of precursor (**Fig. 4**). However, in the case of $NiMo_1W_{11}/Al_2O_3$, the values of *TOF* are much higher than for its counterparts. The increased hydrogenating activity of $NiMo_1W_{11}/Al_2O_3$ can be explained by the high proportion of tungsten; at the same time, high HDS activity and low selectivity in this reaction are characteristic of molybdenum catalysts. Moreover, this nature is not typical for a catalyst prepared from a mixture of two monometallic HPA, which indicates a different nature of the active centers.

3.3 Hydrotreating of SRGO

The characteristics of stable hydrogenation products obtained after hydrotreating of SRGO over $NiMo(W)/Al_2O_3$ catalysts are shown in **Table 4**. The catalytic activity was evaluated by the residual sulfur content in the hydrogenated product. All studied catalysts exhibited stable performance during a 48 hours period. Some catalysts were tested twice, after which the average conversion values of the reagents were calculated. The experiment data show that the accuracy of determining the rate constant is on average 3%. There was no acid component in the catalysts, for this reason no cracking products of model compounds were found in the hydrogenation product. The stable product yield was 96±1%.

The highest residual sulfur content was observed over NiW_{12}/Al_2O_3 catalyst. Replacement of even one tungsten atom by molybdenum (in a stoichiometric ratio) leads to a decrease in the content of sulfur and nitrogen by more than 30% for $Ni(Mo_1+W_{11})/Al_2O_3$ and more than 50% for mixed $NiMo_1W_{11}/Al_2O_3$, which can be explained by the different structure and nature of the active phase. But the lowest content of residual sulfur and nitrogen corresponds to the Mo/(Mo+W) atomic ratio equal to 0.25 for both types of catalysts. The shift in the maximum of HDS activity in comparison with the model feedstock may be

associated with a lower nitrogen content (147 ppm versus 500 ppm) in SRGO. As noted earlier in model reactions, quinoline and their by-products can block the HYD centers, thereby opening vacant HDS centers through anchor adsorption. Since the content of quinoline in SRGO was much lower, inhibition effect was to a lesser extent. As a result, high HYD activity of catalysts with a high molybdenum percentage was observed.

In contrast to HDS (**Fig. 5a**), the HYD function was changed insignificantly with the increase of Mo/W ratio from 3/9 in the catalysts (**Fig. 5b).** Mixed HPAs based samples exhibited higher HYD activity and, as in model reactions without quinoline, no strong effect on the HYD activity was observed with the increase in the fraction of molybdenum in the catalyst. The greatest increase in activity was found when one tungsten atom was replaced by molybdenum. However, at the same time, there is no clearly pronounced dependence of the HYD activity on the atomic ratio of Mo and W for $Ni(Mo_n+W_{12-n})/Al_2O_3$ catalysts. High-efficiency liquid chromatographic analysis of hydrogenated products showed that only bi- and tricyclic aromatic hydrocarbons are hydrogenated, while monocyclic ones underwent almost no transformation.

The degree of removal of nitrogen-containing compounds directly correlates with HDS activity and varied from 73.1 to 91.7% (**Fig. 5c**). NiW_{12}/Al_2O_3 catalyst exhibited the lowest activity. Mixed HPAs based $NiMo_nW_{12-n}/Al_2O_3$ catalysts demonstrated higher activity in HDN reactions during hydrotreating of SRGO than their corresponding counterparts. It should be noted that the peak of the maximum of HDN activity, as in HDS and HYD, refers to the $NiMo_3W_9/Al_2O_3$ catalyst.

4. Characterization

4.1 Characterization of sulfided NiMo(W)/Al_2O_3 catalysts

The textural properties of the liquid phase sulfided samples are summarized in **Table 1**. All catalysts have close textural characteristics. The surface area varied slightly from 202 to 240 m^2g^{-1} and the average pore volume was about 0.5 cm^3g^{-1}. All catalysts had a bimodal pore size distribution with an average diameter of 3.8 nm and 8.4 nm.

Liquid sulfided NiMo(W)/Al_2O_3 catalysts were characterized by HRTEM in order to obtain information about the dispersion of the active phase particles. This is one of the main and traditional methods that allows to obtain the values of dispersion, which is directly correlated with the activity. These dependencies have also been identified in many works [30,43-45]. HRTEM studies allow to obtain general morphological information of individual S–Mo(W)–S particles when the disulfide slabs are oriented parallel to the electron beam. However, this technique does not allow to distinguish between NiMoS, NiWS or NiMoWS slabs due to the lack of a contrast between elements. Typical micrographs, which show the fringes of NiMo(W)S crystallites with 0.65 nm interplanar distances, are presented in **Fig. S1.** The average values of stacking degree and slab length of active phase particles are presented in **Table 5**. For all catalysts, the average length and stacking varied from 3.4 to 4.1 nm and from 1.4 to 2.1, respectively. $NiMo_{12}/Al_2O_3$ had the slabs with the shortest length ~3.4 nm among all studied catalysts and an average stacking number of 1.6, corresponding to high dispersion of the active phase (0.34). NiW_{12}/Al_2O_3 catalyst consisted predominantly of slabs with length ~ 3.9 nm and stacking number ~ 2.1. The introduction of Mo atoms into the composition of the catalysts resulted in a little decrease in average length and average stacking number. The Mo/(Mo+W) atomic ratio had almost no effect on the geometric characteristics of the active phase. By comparison with the active phase morphology of unpromoted catalysts [29], promotion of Mo(W)S_2 phase by Ni decreased the average slab length due to the decorating action of the Ni atoms, which fixed on the edges of Mo(W)S_2 during the formation of the disulfide slabs hindering their further growth. The same effect of promoter atoms on the length of the crystallites was reported in several studies. [46-49]. In addition, Ni-promoted W containing catalysts showed slightly higher stacking degree of slabs than their unpromoted counterparts.

The species formed after liquid phase sulfidation on the surface of the synthesized catalysts have been analyzed by XPS. The XPS spectra of NiMo(W)/Al_2O_3 samples were decomposed in accordance with previously submitted works [25,50]. The spectral region of $Ni2p_{3/2}$ (**Fig. S2**) contains three peaks with their respective satellites. The peak at a BE of 853.7 eV is related to Ni(Mo)WS phase. The signals at 852.9 eV and 856.5 eV correspond to the NiS species and Ni^{2+} in an oxidic environment, respectively

[51-53]. On the Mo3d spectra (**Fig. S3**), there are three doublets corresponding to Mo^{4+} (MoS_2 species) at 229.0 eV and 232.0 eV, the doublet with binding energies at 230.0 and 233.5 eV is related to oxysulfide species and the signals at 232.5 and 235.7 eV is correlated to Mo^{6+} (oxide species). The W 4f spectra (**Fig. S4**) contain three W 4f doublets: the doublet with binding energies at 32.5 and 34.8 eV is associated to W^{4+} species (WS_2 phase), the doublet with binding energies at 33.4 and 35.5 eV to W^{5+} (oxysulfide species), and finally the doublet with binding energies at 36.21 and 38.2 eV to W^{6+} (oxide species). The decomposition of the XPS spectra revealed the relative amount of nickel, molybdenum and tungsten species present on the surface of the sulfided catalysts, summarized in **Table 6**.

In mixed HPA based samples, Mo sulfidation degree, expressed as the percentage of MoS_2 determined by XPS, appears slightly higher than in the corresponding reference samples (less than 10%). In our previous work on the genesis of the active phase in MoW samples, followed *in situ* by Quick-XAS [48], we have evidenced a difference in the sulfidation steps for Mo in MoW and Mo+W samples (in MoW sample, the second sulfidation intermediate appears at lower temperature than in Mo+W sample), which could affect the final sulfidation degree of molybdenum.

The tungsten sulfidation degree was slightly lower than those obtained for molybdenum. The trimetallic catalysts prepared by using mixed MoW HPAs had a W sulfidation degree 10-15 rel. % higher than their analogues based on a mixture of two HPAs. Incorporation of molybdenum atoms into the structure of HPAs led to an increase in W sulfidation rate (5-13 rel. %) compared to NiW_{12} catalyst. On the contrary, corresponding NiMoW references samples demonstrated the lowest W sulfidation degree and the quantity of molybdenum had no effect on tungsten sulfidation rate. In our previous work [54], it has been shown that the introduction of molybdenum in the structure of SiW_{12} HPA leads to simultaneous sulfidation of both Mo and W metals in HPA based catalyst with the formation of mixed Mo-W sulfide slabs. This synergetic effect between W and Mo sulfidation was not found for bimetallic reference based on a mixture of two HPAs.

In the trimetallic catalysts, the fraction of Ni species involved in NiMo(W)S active phase increased with the Mo/W ratio and is larger than that obtained in the NiW sample. This effect was slightly higher

for the catalysts prepared from mixed MoW HPAs. Except for the $NiMo_{12}$ sample, the main species is always NiS (about or more 43% of the Ni relative percentage) together with 5-20% of Ni in oxidic environment. It means that more than 80 % of Ni is sulfided, which may be due to the addition of citric acid introduced in the impregnating solution for the preparation of the oxidic precursors. Citric acid chelates the Ni ions, which results in improving the dispersion of Ni species on the support, decreasing the interaction of the Ni ions with the support and thus improving the sulfidation of Ni [48]. However, the excess of Ni that is not used for promotion is present as a pure NiS species that remain at the surface. At the same time, for catalysts based on mixed HPAs, the fraction of bulk nickel sulfide is slightly higher than for samples $Ni(Mo_n+W_{12-n})/Al_2O_3$, which in turn may be associated to an enhancement of the metallic properties of Mo, which is why Ni atoms are more difficult to incorporate into the structure of the active phase. This also confirms our earlier data that the bond between molybdenum and tungsten is retained even during sulfidation. The high proportion of nickel sulfide is also associated to the type of sulfidation. Eijsbouts et al. [55] noted in their work that Ni is more susceptible to segregation into Ni_2S_3 particles under conditions of liquid-phase sulfidation. The formation of large amounts of nickel sulfide may lead to the blocking of edge active sites. However, separate Ni_2S_3 particles can act as a hydrogen donor and facilitate its spillover on the catalyst surface, which in turn leads to increased activity [56].

4.2 HAADF characterization of gas phase sulfided Ni(Mo)W/Al_2O_3 catalysts

HAADF technique allows to visualize the sulfide slabs with basal planes oriented perpendicularly to the electron beam axis with possible investigation of the relative position of Mo and W atoms in the sulfided particles due to the difference in the Z-number, the intensity being with this technique, proportional to $Z^{1.7}$. Typical HAADF images of sulfided $NiMo_3W_9/Al_2O_3$ and $Ni(Mo_3+W_9)/Al_2O_3$ catalysts are presented in **Fig. 6a** and **b**. The sulfide particles of Ni-promoted catalysts had irregular shapes, as observed in the case of unpromoted samples [25], which is attributed to the interaction with alumina surface. Due to the type of contrast formation in HAADF, heavy tungsten atoms are imaged as brighter spots than lighter molybdenum atoms.

HAADF images of $NiMo_3W_9/Al_2O_3$ show the formation of mixed (Ni)MoWS slabs, in which small agglomerates of Mo atoms were surrounded by W ones. Identification of Mo and W in the slabs is confirmed by the intensity profiles of atoms in a row (**Fig. 6b**), where the ratio of intensities is close to the ratio of $Z^{1.7}$ for W and Mo. Even if mixed MoW slabs are clearly observed in the case of this promoted catalyst, the atomic repartition in a disulfide slab differs from the core-shell structure of unpromoted Mo_3W_9/Al_2O_3 catalyst (sulfided with the same gas phase procedure) containing a whole Mo core [25]. The distribution of Mo and W atoms in the particles of $NiMo_3W_9/Al_2O_3$ is more similar to the one that has been observed for unpromoted Mo_3W_9/Al_2O_3 catalyst sulfided under liquid phase by DMDS [29].

The active phase of $Ni(Mo_3+W_9)/Al_2O_3$ sulfided under gas phase consisted mainly of homogeneous (Ni)MoS and (Ni)WS slabs. However, the presence of some mixed (Ni)MoWS slabs was also evidenced. Thus, the structure of sulfide particles in $Ni(Mo_3+W_9)/Al_2O_3$ catalyst is quite similar to the one observed for unpromoted $(Mo_3+W_9)/Al_2O_3$ sample sulfided under gas or liquid phase [25].

HAADF results unambiguously show the formation of mixed particles (Ni)MoWS in promoted mixed HPA based catalyst with a random distribution of Mo inside the WS_2 slabs. In contrast, the predominance of (Ni)MoS and (Ni)WS particles with a small number of mixed slabs is observed in the case of promoted catalyst prepared from a mixture of two monometallic HPAs.

4.3 EXAFS characterization of gas phase sulfided Ni(Mo)W/Al_2O_3 catalysts

Liquid phase sulfidation before catalytic tests was chosen to be close to the real conditions of hydrotreating reactions, as a consequence, the same type of activation was used to obtain the general information of morphology and content of active phase. It is complicated to make a distinction between a mixed $MoWS_2$ phase and a mixture of monometallic ones and the techniques with atomic resolution are needed. For this reason, EXAFS characterization was done. Unfortunately, the instrumentation on the beam line and construction of the cell did not allow at this stage using liquid phase sulfidation, so to avoid reoxidation the samples were sulfided *in situ* in the gas phase. To support and supplement EXAFS data, the HAADF characterization was also done after gas phase sulfidation.

Previously, we have shown that for the unpromoted MoW systems prepared from mixed HPA, the main impact of the sulfidation type (DMDS vs H_2S/H_2) was on the structure of mixed $MoWS_2$ particles [25]: a core-shell distribution of Mo and W is observed in the case of gas phase sulfidation while a more random distribution of the atoms is evidenced in the case of liquid phase sulfidation. Regardless of the activation type, mixed HPA based catalysts had high amount of mixed $MoWS_2$ clusters, while samples based on a mixture of two monometallic HPAs had predominantly monometallic MoS_2 and WS_2 slabs. In the present work, the main task of HAADF and EXAFS characterization was to determine how the addition of nickel to MoW systems affected the formation of active phase, the promotion effect being expected to be the same under gas or liquid phase sulfidation, despite possible differences in the location of Mo and W atoms inside the slabs.

EXAFS characterization was aimed at determining the nature of the sulfide species in the sulfided $NiMo(W)/Al_2O_3$ catalysts. Trimetallic $NiMo_3W_9/Al_2O_3$ catalyst was chosen as it is the most effective in model HDS, HYD and HDN reactions as well as in SRGO HDT. **Fig. 7** compares the magnitude of k^3-weighted Fourier transformed (FT) EXAFS spectra for bimetallic $NiMo_{12}/Al_2O_3$ (NiW_{12}/Al_2O_3) and trimetallic $NiMo_3W_9/Al_2O_3$ and $Ni(Mo_3+W_9)/Al_2O_3$ catalysts. The best-fit parameters for EXAFS data are gathered in **Table 7**. At both Mo *K*- and W L_3-edges, the first FT contribution with a maximum at 2.0 Å (not phase corrected) was attributed to the metal-sulfur first coordination. The coordination numbers of the Mo−S and W−S contributions varied from 5.4 to 6.1 for all studied samples, thus indicating the high sulfidation degree of metals (**Table 7**).

The contribution around 2.9 Å (not phase corrected) at both edges was assigned to metal backscatter within $Mo(W)S_2$ structure. A noticeable decrease can be seen in the second coordination shell when comparing trimetallic samples to bimetallic NiMo and NiW references (**Fig. 7**), particularly for mixed HPA based catalyst. The same behavior was already observed for unpromoted samples [57], the second coordination shell was more modified for the catalysts prepared from Mo_3W_9 HPA compared to those based on a mixture of two monometallic HPAs. In the bimetallic catalysts, the coordination numbers were $N_{Mo\text{-}Mo}$ = 3.7 (at 3.18 Å) for $NiMo_{12}/Al_2O_3$ and $N_{W\text{-}W}$ = 4.3 (at 3.16 Å) for NiW_{12}/Al_2O_3.

The higher value for W−W compared to Mo−Mo can be related to larger sulfide particles in NiW_{12} sample, which is in agreement with TEM data.

For both trimetallic catalysts, the fit at the Mo *K*-edge was improved when adding a second metal-metal Mo−W contribution in the second coordination shell. The second coordination shell at the Mo *K*-edge in $NiMo_3W_9/Al_2O_3$ consists of a molybdenum atom with $N_{Mo\text{-}Mo} = 1.5$ and a tungsten one with $N_{Mo\text{-}W} = 2.8$, in $Ni(Mo_3+W_9)/Al_2O_3$ with $N_{Mo\text{-}Mo} = 3.3$ and $N_{Mo\text{-}W} = 1.6$ both at 3.19 Å. The simultaneous presence of Mo−Mo and Mo−W contributions indicates the formation of mixed sulfide phase in both NiMoW catalysts. However, the higher contribution of Mo−W path for the second shell in $NiMo_3W_9/Al_2O_3$ indicates the higher concentration of mixed slabs than in its trimetallic $Ni(Mo_3+W_9)/Al_2O_3$ counterpart. Indeed, a comparison of trimetallic catalysts by HAADF shows that both samples contain mixed $MoWS_2$ particles but in $Ni(Mo_3+W_9)/Al_2O_3$ these mixed slabs are less numerous.

At the W L_3-edge of trimetallic samples, a lower W−W coordination number is observed, compared to that of NiW_{12} catalyst. The morphology of WS_2 slabs could thus be affected by the presence of Mo. The same evolution of the coordination numbers was also observed for the corresponding unpromoted catalysts showing that the behavior does not depend on the Ni promotion [57]. The second coordination shell of trimetallic samples contains one heteroatomic metal-metal contribution. It should also be noticed that tungsten concentration was three times higher than molybdenum. Thus, the obtained distribution of the contributions may be indicative of a greater presence of tungsten atoms surrounding small molybdenum islands, which have more W neighbors in this case. That is in agreement with the results of HAADF characterization.

The characterizations under gas phase sulfidation have proven that the Ni promotion of the MoW catalysts does not inhibit the formation of the mixed $MoWS_2$ slabs when the oxidic precursor contains both Mo and W atoms.

Determination of the local environments of the Ni atoms in the sulfided catalysts from the EXAFS data is hampered. In sulfided catalyst nickel could be part of various compounds, such as Ni_3S_2, NiS_x,

and NiMo(W)S phase. Such multicomponent system presents different scattering paths overlapping in the *R*-range, which leads to instability of the fitting procedure and correlations of the fitting parameters.

The Ni *K*-edge XANES and EXAFS spectra of sulfided catalysts are shown in **Fig. 8A** and **B**, respectively. For comparison purposes, Ni/Al_2O_3 catalyst was also synthesized using impregnating solutions prepared from a mixture of nickel carbonate and citric acid with molar ratio citric acid/Ni = 1/1. This sample was gas-phase sulfided under the same conditions as $Ni(Mo)W/Al_2O_3$ catalysts and its XAS spectra were also recorded.

All Ni *K*-edge EXAFS spectra are similar in phase (**Fig. 8B**). The oscillations of the Ni−S scattering will dominate in the lower *k*-region with a characteristic maximum around 6 $Å^{-1}$ corresponding to the maximum of the scattering amplitude of S backscatters, whereas Mo and W backscatters will contribute at the higher *k*, leading when they are coordinated as second neighbors of promotors to a second relative maximum beyond 10 $Å^{-1}$ [58,59]. For the bimetallic and trimetallic catalysts, this second relative maximum is observed in agreement with the decoration of the sulfide slabs by nickel atoms. It is noteworthy that both trimetallic catalysts (**Fig. 8B (b)**) display a maximum at higher *k*, which is markedly lower in intensity than the ones observed for the bimetallic catalysts (**Fig. 8B (a)**). This decrease of signal in the higher *k*-region is in agreement with the simultaneous presence of W and Mo, which is due to the destructive interference of the individual scattering paths of these atoms, which are out of phase [11,62].

The Ni *K*-edge XANES spectra of the $NiMo(W)/Al_2O_3$ catalysts differ from Ni/Al_2O_3 due to the changes in the electronic structure by the appearance of Mo and/or W neighbors (**Fig. 8A (a),(b)**). Spectra of both trimetallic catalysts are close to each other (**Fig. 8A (b)**). The spectrum of mixed HPA based sample looks like an intermediate between its trimetallic counterpart and $NiMo_{12}/Al_2O_3$ sample (**Fig. 8A (c)**), while $Ni(Mo_3+W_9)/Al_2O_3$ itself is close to the NiW_{12}/Al_2O_3 (**Fig. 8A (d)**).

Summarizing, the XAS data showed that the promotion by Ni does not prevent the formation of mixed MoWS sulfide phase in trimetallic catalysts. These mixed slabs are formed with Mo islands surrounded by W atoms. However, the active phase of the catalyst prepared from separate

monometallic HPAs consisted mainly of monometallic sulfide particles. The changes of the Ni *K*-edge XANES spectra indicate the formation of NiMo(W)S phase along with nickel sulfide.

5. Discussion

The results of testing the catalysts in hydrotreating of DBT and naphthalene showed that not only the atomic ratio of structure-forming Mo and W metals, but also the type of precursor affects the catalytic activity. The high activity of mixed HPAs based $NiMo_nW_{12-n}/Al_2O_3$ catalysts is related to the proximity of Mo and W atoms in starting material and results in a synergetic effect between them after sulfidation through the formation of mixed Ni promoted $MoWS_2$ slabs that was confirmed by the results of EXAFS and HAADF characterization. It should be taken into account that the use of mixed HPAs leads to a high sulfidation of metals and more efficient incorporation of nickel into the active phase, according to the XPS results (**Table 6**) and as a consequence, to higher catalytic performances in model feed and SRGO hydrotreating (**Figs. 1, 2 and 5**).

The introduction of quinoline influences greatly the hydrogenating activity in the model reactions [42,62], which was also found in the present work (**Fig. 2**). The mechanism of the effect of nitrogen-containing compounds on the hydrogenolysis of DBT was previously described in the literature [62,63]. It was shown that the tetrahydroquinoline formed as a main product of the reaction, being adsorbed perpendicular to the catalyst surface on one π-active site, leaves the second vacant active site available for anchor σ-adsorption of the DBT molecule, thereby shifting the reaction to the direct desulfurization route. This effect explains the increase in HDS activity in model reactions upon the addition of quinoline. Kinetic studies using model compounds presented in [64,65] also confirm the assumption that nitrogen-containing heterocyclic compounds inhibit to a greater extent the HYD route of the DBT HDS.

It is known that hydrotreating catalysts based on NiWS have high catalytic activity in HYD and HDN reactions especially at severe conditions while NiMoS based ones show high activity in HDS [66, 67]. The obtained dependences (**Fig. 1-3**) indicate that changing the Mo/(Mo+W) atomic ratio leads to change the ratio between HDS and HYD. Our results show that this ratio is not directly associated with the geometric characteristics of the active phase particles – length and stacking (**Table 5**), but could

depend on the specific location of molybdenum and tungsten atoms in the crystallite structure. Different inhibition behaviors were noticed depending on the Mo/W ratio in the catalysts and on the precursor used. Thus, tungsten-rich catalysts are less sensitive to the presence of quinoline in DBT HDS and naphthalene HYD (**Fig. 3c**). All mixed HPAs based catalysts are more resistant to inhibition than their trimetallic counterparts.

TOF_{edge} values decrease with an increase in the fraction of molybdenum, consequently for mixed $NiMo_nW_{12-n}/Al_2O_3$ catalysts, higher *TOF* values are observed at low Mo/W ratio. An increase of the Mo/(Mo+W) atomic ratio from 0.25 leads to an equalization of hydrogenation activity between the $NiMo_nW_{12-n}/Al_2O_3$ and $Ni(Mo_n+W_{12-n})/Al_2O_3$ systems, which indicates the similar nature of the edge sites (**Fig. 4**). For a more detailed analysis of the Ni-promoting effect, the values of promotion degree $(Ni/(Mo+W)_{edge})$ of $Mo(W)S_2$ crystallite edges were calculated based on XPS and TEM data [7,20]. The $Ni/(Mo+W)_{edge}$ values varied from 0.79 to 0.98. As noted earlier, the sulfidation degree increases with molybdenum percentage in the active phase. Incorporation of nickel atoms was easier in catalysts based on two monometallic HPAs, which can be explained by a presence of separate MoS_2 species. In order to assess the influence of the main factors, the 3D dependences of TOF_{edge} in DBT HDS during co-hydrotreating of DBT, naphthalene and quinoline on the Ni-promoting degree and the Mo/(Mo+W) atomic ratio were constructed (**Fig. 9**). It was found that the ratio of structure-forming metals plays a key role in changing the activity of the edge centers while the degree of promotion had significantly less impact.

The high TOF of tungsten-rich catalysts can be explained by their good resistance to poisoning with nitrogen-containing compounds (**Fig. 3**).

In the case of naphthalene HYD there is a correlation between HYD rate constants and the amount of Ni in NiMo(W)S phase except for NiW_{12}/Al_2O_3 (**Fig. S6**), which was more active than one might expect. The $NiMo_1W_{11}/Al_2O_3$ catalyst offers 1.4 times better HYD activity in the presence of quinoline. Observed results might indicate that in this case hydrogenation sites could be different from the HDS sites (relative to DDS pathway) and that hydrogenation activity is linked to Ni atoms in promoting sites

independently of NiMoS, NiWS, and also mixed NiMoWS sites, the activity level of each hydrogenation site being leveled by the presence of Ni. These results witness some differences in synergy effect between Ni and mixed sulfide phase mainly present in mixed HPA catalysts.

Regarding catalytic behavior of trimetallic systems in HDS of SRGO, the most important and significant results were observed. All NiMoW catalysts showed at least 1.2 times higher k_{HDS} values than predicted additive ones regardless of the type of starting oxide precursor (**Fig. 5a**). Even if trimetallic reference catalysts based on two HPAs are slightly less efficient than MoW HPAs based ones they are still more active than bimetallic samples. The results present some differences in synergy effect between Ni and mixed sulfide phase mainly present in mixed HPAs catalysts and show the advantage of the use of ternary catalysts over NiMo and NiW systems. The low nitrogen content in the SRGO compared to model N-containing feed resulted in less inhibition of molybdenum-containing catalysts, thereby shifting the maximum HDS and HDN activity from $NiMo_1W_{11}/Al_2O_3$ to $NiMo_3W_9/Al_2O_3$ sample with a higher molybdenum content (**Fig. 5**). For both types of catalysts, HYD and HDN activities present the same evolution, which was also reported earlier [63]. It should also be noted that synthesized catalysts based on the mixed Keggin-type HPAs have higher activity values compared to their analogues, which is associated to the formation of a larger quantity of highly active mixed NiMoWS phase due to the closer interaction of metals in the precursor, according to EXAFS and HAADF data.

It was previously noted by Lercher and co-workers [68] that the hydrogenating activity correlated with concentration of SH-groups formed due to the dissociative adsorption of H_2 and H_2S. In another work [69], investigating catalytic activity of unsupported trimetallic NiMoW systems, the authors found by using the method of continuous-flow H_2-D_2 scrambling, that the concentration of SH-groups directly depends on the tungsten content in mixed NiMoW systems. This can explain the highest HDS, HYD and HDN activities of the $NiMo_1W_{11}/Al_2O_3$ and $NiMo_3W_9/Al_2O_3$ samples in model reactions and SRGO HDT (**Figs. 1, 2, 5**) and enhanced inhibition resistance (**Fig. 3**).

Table 8 presents the results of various research groups in the area of investigation on Mo and W synergistic effects for NiMoW bulk and supported catalysts. In most works, both for bulk and supported

catalysts, a positive effect was found when using Ni-promoted mixed MoW systems [5,22,70,71]. However, there are publications in which this effect was observed only in some cases [11].

Raybaud and his co-workers [22] using DFT calculations found that the high activity of the $NiMo_{0.5}W_{0.5}S$ catalyst is explained by an optimal energy of the metal-sulfur bond at the edges of the active phase compared with that in bimetallic NiMoS and NiWS systems, which was also confirmed by catalytic tests in the thiophene HDS.

Olivas et al [70] using extended Huckel methods found that the combination of Mo and W atoms in mixed bulk catalysts changes the semiconductor behavior and increases the metallic character of MoS_2 or WS_2. Moreover, the additional promotion by Ni further increases the availability of electrons over the Fermi level. It was found that the greatest effect is achieved with a Mo/(Mo+W) ratio of 0.85. This effect was associated to the formation of more optimal mixed (Ni)MoWS phase, which is mentioned in a number of other later works [12,72]. It should be said that no similar synergistic effect was found for the Co-promoted systems. Similar dependences were obtained for supported catalysts in DBT HDS and hydrotreating of vacuum gas oil by Tomina et al [73]. Investigating the influence of the ratio of the structure-forming metals of the active phase, it was found that the maximum HDS activity was achieved at a ratio of Mo/W = 1/1. The high activity of the trimetallic $NiMoW/Al_2O_3$ catalyst was also associated to the optimal M-S binding energy in [74], where it was also noted that the addition of Ni and Mo to WO_x-modified Al_2O_3 provides a strong interaction between NiO and MO_x particles, which facilitates their reduction.

Shan et al. [5] attributed the high activity of $NiMoW/Al_2O_3$ catalysts to the close interaction of metals and ability to generate highly dispersed W/Mo/Ni oxide species, due to which the metals are better reduced, and therefore sulfided. The authors also noted in their work that the precursor has a direct effect on the interaction of metals.

Interesting results were obtained by Hensen et al. [11] The authors investigated the influence of the Mo/(Mo+W) ratio and the sulfidation conditions on the composition and structure of the active phase in trimetallic alumina supported catalysts. Using the EXAFS method, it was found that, depending on

the sulfiding conditions, a mixed active phase with a different structure can be formed. Under gas phase sulfidation at 1 bar, a mixed phase with a "core-shell" structure (a molybdenum core surrounded by tungsten atoms) was predominantly formed. An increase in pressure (up to 15 bar) or temperature (from 400 to 650ºC) leads to disordering and formation of a structure with a random distribution of Mo and W atoms. A synergistic effect was established for the $NiMo_{0.75}W_{0.25}/ Al_2O_3$ catalyst in hydrotreating of gas-oil (234 ppm of nitrogen), while the effect was not observed in the model reactions of HDS of DBT and thiophene. The authors suggested that the mixed catalysts may have enhanced hydrogenation activity, while the hydrogenolysis activity is unaffected, which is also consistent with other works [71,74,75].

Summarizing the results obtained in this present work and literature data, we can note the following relationships. Trimetallic NiMoW systems have a higher hydrogenating activity, apparently due to the formation of a greater number of SH-groups. The maximum hydrogenating activity was achieved with a low Mo/W metal ratio in the mixed NiMoW catalyst. The composition of trimetallic NiMoW catalysts should be selected in accordance with the composition of the feed and the amount of N-containing compounds having a direct effect on the ratio of HYD and HDS performances. The Mo (W) precursor plays a key role in the creation of high active alumina supported (Ni)MoWS mixed catalytic systems. The use of mixed MoW-HPAs made it possible to significantly increase the synergistic effect between Mo and W due to the formation of a larger amount of a mixed NiMoWS active phase.

The possible modification of acidic properties of the catalysts due to the presence of silica in the HPA was not considered since the Si content was the same in all prepared samples. Earlier several works were devoted to explaining the role of heteroatoms in the Keggin structure of HPA for HDT catalysts. Thus, in [76] CoMo catalysts based on $SiMo_{12}$ and PMo_{12} HPAs were compared with those prepared from ammonium heptamolybdate, in [77] PMo_{12} and PW_{12} HPAs were used as precursors for NiMo(W) catalysts as an alternative to ammonium heptamolybdate and ammonium metatungstate. The authors concluded that the main effect on catalytic activity is exerted by the structure of Keggin HPAs, and not the nature of the heteroatom (Si or P). Taking into account the results, we suppose that Si atoms are located on the alumina surface without significant changes of acidity and HDT performance. However,

this does not mean that silicon or phosphorus has no effect on hydrotreating catalysts. The way of synthesis of P-modified tri-metallic NiMoW/Al_2O_3 catalysts had a dramatic impact on structure of active phase species and catalytic activity [78]. Incorporation of phosphorus weakened the metal-support interactions and facilitated the formation of more synergetic NiWMoS phases with higher stacks. However, these changes were positive effect on fluid catalytic cracking diesel hydrofining only in case of WMoNi/Al_2O_3 catalyst prepared using W/Mo-hybrid nanocrystal-assisted hydrothermal deposition method compared to tri-metallic reference obtained using conventional precursors and incipient impregnation technique.

6. Conclusions

In the present work, NiMoW catalysts supported on alumina were prepared by co-impregnation of nickel carbonate, citric acid and mixed $SiMo_nW_{n-12}$ (n = 1, 3, 6 and 9) HPAs and characterized by different techniques. Trimetallic reference Ni(Mo_n+W_{12-n})/Al_2O_3 catalysts were also synthesized from a mixture of two monometallic $SiMo_{12}$ and SiW_{12} HPAs with the same Mo/W ratio as in the mixed HPAs based catalysts.

HAADF and XAS characterizations performed after gas phase sulfidation of trimetallic solids with the (Mo/Mo+W) ratio equal to 0.25 have allowed to evidence the formation of promoted mixed $MoWS_2$ slabs, where isolated Mo islands are randomly distributed inside the WS_2 slabs for the catalyst prepared from $SiMo_3W_9$ HPA while the active phase of the catalysts based on two separate HPAs consisted mainly of monometallic sulfide slabs. The behavior of the promoted samples towards the formation of the sulfide slabs is similar to that observed with unpromoted ones [25] specially showing that the presence of nickel does not hinder the formation of mixed clusters in HPA based catalysts.

Liquid sulfided NiMo(W)/Al_2O_3 catalysts were characterized by XPS and HR-TEM. XPS analysis allows estimating the amount of Ni-promoted $MoWS_2$ phase, which was ca. 10 % higher compared to NiW_{12}/Al_2O_3 reference catalyst. Tungsten sulfidation degree in the $NiMo_nW_{12-n}/Al_2O_3$ catalysts was higher compared to the corresponding counterparts, which can be related to the simultaneous sulfidation of Mo and W due to their proximity in the initial MoW-heteropolyanion precursor. The dispersion values

obtained by the TEM results indicate that the type of precursor does not affect the distribution of the $NiMo(W)S_2$ active phase particles over the support surface. Disulfide crystallites were mainly represented by single- and two-layer particles. The calculated $Ni/(Mo+W)_{edge}$ values showed that the atomic ratio does not significantly affect the degree of promotion.

Catalytic tests were performed using liquid phase sulfidation in a bench scale flow reactor. $NiMo_1W_{11}/Al_2O_3$ and $NiMo_3W_9/Al_2O_3$ samples demonstrated the highest HDS, HYD and HDN activities in model feed (DBT, naphthalene with addition of quinoline) and SRGO HDT. Three-dimensional (TOF_{edge} vs Mo/(Mo+W) atomic ratio vs $Ni/(Mo+W)_{edge}$) dependences showed that the Mo/W atomic ratio of the structure-forming metals in the active phase has the greatest effect on the catalytic activity of the catalysts. Enhanced N-inhibition resistance was observed at a low Mo/W ratio. High activity of mixed HPAs based $NiMo_nW_{12-n}/Al_2O_3$ catalysts associates with the proximity of Mo and W atoms in starting material and results in a synergetic effect between them after sulfidation through the formation of mixed promoted $MoWS_2$ slabs that was confirmed by EXAFS and HAADF results. The Mo/(Mo+W) ratio in the catalysts should be selected depending on the content of N-containing compounds in the feed. For petroleum fractions with a high nitrogen content, blended NiMoW catalysts with a high tungsten content are most preferred due to their higher resistance to inhibition effect.

Acknowledgments

The authors thank Russian Science Foundation for financial support of theoretical part of the investigation by Grant No. 17-73-20386. The preparation and testing parts have been supported by the Government of Russian Federation (decree №220 of April 9, 2010), agreement №14.Z50.31.0038. The authors thank the Chevreul Institute (FR 2638) for its help in the development of this work. Chevreul Institute is supported by the «Ministère de l'Enseignement Supérieur et de la Recherche», the «Région Nord-Pas de calais» and the «Fonds Européen de Développement des Régions». This work was supported by a public grant overseen by the French National Research Agency (ANR) as part of the

1 “Investissements d’Avenir” program (reference: ANR-10-EQPX-45) and provided for the building and
2 operation of the ROCK beamline (SOLEIL, France).

3

References

[1] R. Suarez-Bertoa, M. Pechout, M. Vojtíšek, C. Astorga, Regulated and Non-Regulated Emissions from Euro 6 Diesel, Gasoline and CNG Vehicles under Real-World Driving Conditions // Atmosphere. 11(2) (2020) 204.

[2] Q. Meng, P. Du, A. Duan, Z. Zhao, J. Liu, D. Shang, D. Hu, Trimetallic Catalyst Supported Zirconium-Modified Three-Dimensional Mesoporous Silica Material and Its Hydrodesulfurization Performance of Dibenzothiophene and 4,6-Dimethydibenzothiophene // Ind. Eng. Chem. Res. 59 (2020) 654−667.

[3] J. Hein, O. Y. Gutiérrez, S. Albersberger, J. Han, A. Jentys, J. A. Lercher, Towards Understanding Structure–Activity Relationships of Ni–Mo–W Sulfide Hydrotreating Catalysts // Chem. Cat. Chem. 9(4) (2016) 629–641.

[4] Y. Liu, B. Xu, B. Qin, C. Tao, L. Cao, Y. Shen, Novel NiMoW-clay hybrid catalyst for highly efficient hydrodesulfurization reaction // Catal. Commun. 144 (2020) 106086.

[5] S. Shan, H. Liu, Y. Yue, G. Shi, X. Bao, Trimetallic WMoNi diesel ultra-deep hydrodesulfurization catalysts with enhanced synergism prepared from inorganic–organic hybrid nanocrystals // J. Catal. 344 (2016) 325-333.

[6] M. Corral Valero, P. Raybaud, Computational chemistry approaches for the preparation of supported catalysts: Progress and challenges // J. Catal. 391 (2020) 539-547.

[7] A. V. Mozhaev, P. A. Nikulshin, Al. A. Pimerzin, K. I. Maslakov, A. A. Pimerzin, Investigation of co-promotion effect in NiCoMoS/Al_2O_3 catalysts based on Co_2Mo_{10}-heteropolyacid and nickel citrate // Catal. Today 271 (2016) 80-90.

[8] P. A. Nikulshin, N. N. Tomina, A. A. Pimerzin, A. Yu. Stakheev, I. S. Mashkovsky, V. M. Kogan, Effect of the second metal of Anderson type heteropolycompounds on hydrogenation

and hydrodesulphurization properties of $XMo_6(S)/Al_2O_3$ and Ni_3-$XMo_6(S)/Al_2O_3$ catalysts // Appl. Catal. A 393 (2011) 146-152.

[9] S. L. Amaya, G. Alonso-Núñez, T. A. Zepeda, S. Fuentes, A. Echavarría, Effect of the divalent metal and the activation temperature of NiMoW and CoMoW on the dibenzothiophene hydrodesulfurization reaction // Appl. Catal. B 148–149 (2014) 221–230.

[10] Y. Yi, B. Zhang, X. Jin, L. Wang, C. T. Williams, G. Xiong, D. Su, C. Liang, Unsupported NiMoW sulfide catalysts for hydrodesulfurization of dibenzothiophene by thermal decomposition of thiosalts // J. Mol. Catal. A: Chem. 351 (2011) 120–127.

[11] L. van Haandel, M. Bremmer, P. J. Kooyman, J. A. Rob van Veen, T. Weber, E. J. M. Hensen, Structure–Activity Correlations in Hydrodesulfurization Reactions over Ni-Promoted $Mo_xW_{(1-x)}S_2/Al_2O_3$ Catalysts // ACS Catalysis 5 (2015) 7276-7287.

[12] D. M. Nejad, N. Rahemi, S. Allahyari, Effect of tungsten loading on the physiochemical properties of nanocatalysts of Ni–Mo–W/carbon nanotubes for the hydrodesulfurization of thiophene // Reac. Kinet. Mech. Cat. 120 (2017) 279-294.

[13] A. Kokliukhin, M. Nikulshina, A. Mozhaev, C. Lancelot, P. Blanchard, O. Mentré, P. Nikulshin, The effect of the Mo/W ratio on the catalytic properties of alumina supported hydrotreating catalysts prepared from mixed $SiMo_6W_6$ and $SiMo_9W_3$ heteropolyacids // Catal. Today (2020) doi:10.1016/j.cattod.2020.07.050.

[14] W. Qian, Y. Hachiya, D. Wang, K. Hirabayashi, A. Ishihara, T. Kabe, H. Okazaki, M. Adachi, Elucidation of promotion effect of nickel on Mo/Al_2O_3 and Co-Mo/Al_2O_3 catalysts in hydrodesulfurization using a ^{35}S radioisotope tracer method // Appl. Catal. A 227 (2002) 19-28.

[15] M. Mashayekhi, S. Soltanali, S. R. S. Mohadecy, M. Rashidzadeh, Activity Study of NiMoW, NiCoMo Trimetallic Catalysts for Heavy Gas Oil Hydrotreating // Pet. Chem. 60(7) (2020) 785–793.

[16] T. K. T. Ninh, D. Laurenti, E. Leclerc, M. Vrinat, Support effect for CoMoS and CoNiMoS hydrodesulfurization catalysts prepared by controlled method // Appl. Catal. A 487 (2014) 210-218.

[17] J. A. Medina Cervantes, R. Huirache-Acuña, J. N. Díaz de León, S. Fuentes Moyado, F. Paraguay-Delgado, G. Berhault, G. Alonso-Núñez, $CoNiMo/Al_2O_3$ sulfide catalysts for dibenzothiophene hydrodesulfurization: Effect of the addition of small amounts of nickel // Micropor Mesopor Mat. 309 (2020) 110574.

[18] L. Medici, R. Prins, The Influence of Chelating Ligands on the Sulfidation of Ni and Mo in $NiMo/SiO_2$ Hydrotreating Catalysts // J. Catal. 163 (1996) 38-49.

[19] M. S. Rana, J. Ramírez, A. Gutiérrez-Alejandre, J. Ancheyta, L. Cedeño, S. K. Maity, Support effects in CoMo hydrodesulfurization catalysts prepared with EDTA as a chelating agent // J. Catal. 246 (2007) 100-108.

[20] P. A. Nikulshin, D. I. Ishutenko, A. A. Mozhaev, K. I. Maslakov, A. A. Pimerzin, Effects of composition and morphology of active phase of $CoMo/Al_2O_3$ catalysts prepared using Co_2Mo_{10}–heteropolyacid and chelating agents on their catalytic properties in HDS and HYD reactions // J. Catal. 312 (2014) 152-169.

[21] A. V. Mozhaev, M. S. Nikul'shina, C. Lancelot, P. Blanchard, C. Lamonier, P. A. Nikul'shin, Trimetallic Hydrotreating Catalysts $CoMoW/Al_2O_3$ and $NiMoW/Al_2O_3$ Prepared on the Basis of Mixed Mo-W Heteropolyacid: Difference in Synergistic Effects // Pet. Chem. 58 (2018) 1198-1205.

[22] C. Thomazeau, C. Geantet, M. Lacroix, M. Danot, V. Harlé, P. Raybaud, Predictive approach for the design of improved HDT catalysts: γ-Alumina supported (Ni, Co) promoted $Mo_{1-x}W_xS_2$ active phases // Appl. Catal. A 322 (2007) 92–97.

[23] R. Huirache-Acuña, B. Pawelec, C. V. Loricera, E. M. Rivera-Mu˜noz, R. Nava, B. Torres, J. L. G. Fierro, Comparison of the morphology and HDS activity of ternary Ni(Co)-Mo-W catalysts supported on Al-HMS and Al-SBA-16 substrates // Appl. Catal. B 125 (2012) 473-485.

[24] Y. E. Licea, R. Grau-Crespo, L. A. Palacio, A. C. Faro Jr., Unsupported trimetallic Ni(Co)-Mo-W sulphide catalysts prepared from mixed oxides: Characterisation and catalytic tests for simultaneous tetralin HDA and dibenzothiophene HDS reactions // Catal. Today 292 (2017) 84–96.

[25] M. Nikulshina, A. Mozhaev, C. Lancelot, P. Blanchard, M. Marinova, C. Lamonier, P. Nikulshin, Enhancing the hydrodesulfurization of 4,6-dimethyldibenzothiophene through the use of mixed $MoWS_2$ phase evidenced by HAADF // Catal. Today 329 (2019) 24-34.

[26] J. Hein, O. Y. Gutiérrez, E. Schachtl, P. Xu, N. D. Browning, A. Jentys, J. A. Lercher, Distribution of Metal Cations in Ni-Mo-W Sulfide Catalysts // Chem. Cat. Chem. 7 (2015) 3692–3704.

[27] G. An, C. Liu, C. Xiong, C. Lu, A Study on the Morphology of Unsupported Ni-Mo-W Sulfide Hydrotreating Catalysts Through High-resolution Transmission Electron Microscopy // Pet. Sci. Technol. 30 (2012) 1599–1608.

[28] J. A. Mendoza-Nieto, O. Vera-Vallejo, L. Escobar-Alarcón, D. Solís-Casados, T. Klimova, Development of new trimetallic NiMoW catalysts supported on SBA-15 for deep hydrodesulfurization // Fuel 110 (2013) 268–277.

[29] M. Nikulshina, A. Mozhaev, C. Lancelot, M. Marinova, P. Blanchard, E. Payen, P. Nikulshin, MoW synergetic effect supported by HAADF for alumina based catalysts prepared from mixed $SiMo_nW_{12-n}$ heteropolyacids // Appl. Catal. B 224 (2018) 951–959.

[30] S. Kasztelan, H. Toulhoat, J. Grimblot, J.P. Bonnelle, A geometrical model of the active phase of hydrotreating catalysts // Appl. Catal. 13 (1984) 127-159.

[31] E. J. M. Hensen, P. J. Kooyman, Y. van der Meer, A.M. van der Kraan, V. H. J. de Beer, J. A. R. van Veen, R. A. van Santen, The Relation between Morphology and Hydrotreating Activity for Supported MoS_2 Particles // J. Catal. 199 (2001) 224-235.

[32] K. B. Tayeb, C. Lamonier, C. Lancelot, M. Fournier, A. Bonduelle-Skrzypczak, F. Bertoncini, Active phase genesis of NiW hydrocracking catalysts based on nickel salt heteropolytungstate: Comparison with reference catalyst // Appl. Catal. B 126 (2012) 55–63.

[33] V. Briois, C. La Fontaine, S. Belin, L. Barthe, T. Moreno, V. Pinty, A. Carcy, R. Girardot, E. Fonda, ROCK: the new Quick-EXAFS beamline at SOLEIL // J. Phys. Conf. Ser. (JPCS). 712 (2016) 1–6.

[34] C. La Fontaine, L. Barthe, A. Rochet, V. Briois, X-ray absorption spectroscopy and heterogeneous catalysis: Performances at the SOLEIL's SAMBA beamline // Catal. Today 205 (2013) 148-158.

[35] B. Ravel, M. Newville, ATHENA, ARTEMIS, HEPHAESTUS: data analysis for X-ray absorption spectroscopy using IFEFFIT // J. Synchrotron Radiat. 12 (2005) 537–541.

[36] Z. Liu, W. Han, D. Hu, S. Sun, A. Hu, Z. Wang, Y. Jia, X. Zhao, Q. Yang, Effects of Ni–Al_2O_3 interaction on NiMo/Al_2O_3 hydrodesulfurization catalysts // J. Catal. 387 (2020) 62–72.

[37] M. Lewandowski, Z. Sarbak, Simultaneous HDS and HDN over supported PtSn catalysts in comparison to commercial NiMo/Al2O3 // Appl. Catal. B: Environ. 79 (2008) P. 313

[38] J. Ancheyta, M. J. Angeles, M. J. Macias, G. Marroquin, R. Morales, Changes in Apparent Reaction Order and Activation Energy in the Hydrodesulfurization of Real Feedstocks // Energ Fuel 16 (2002) 189-193.

[39] J. L. García-Gutiérrez, G. C. Laredo, G. A. Fuentes, P. García-Gutiérrez, F. Jiménez-Cruz, Effect of nitrogen compounds in the hydrodesulfurization of straight-run gas oil using a CoMoP/g-Al_2O_3 catalyst // Fuel 138 (2014) 98–103.

[40] S. K. Bej, R. P. Dabral, P. C. Gupta, K. K. Mittal, G. S. Sen, V. K. Kapoor, A. K. Dalai, Studies on the Performance of a Microscale Trickle Bed Reactor Using Different Sizes of Diluent // Energ Fuel 14 (2000) 701–705.

[41] C. Marín, J. Escobar, E. Galván, F. Murrieta, R. Zárate, V. Cortés, NiMo Supported on Faujasite-modified Al_2O_3 as Catalysts for the Hydrotreatment of a Light Cycle Oil/Straight Run Gas Oil Mixture // Can. J. Chem. Eng. 80 (2008) 903–910.

[42] M. Egorova, R. Prins, Mutual influence of the HDS of dibenzothiophene and HDN of 2-methylpyridine // J. Catal. 221(1) (2004) 11–19.

[43] R. Guo, B. Shen, X. Fang, J. Sun, C. Peng, X. Cui, A study on the relationship between the active phase microstructure and hydrodesulfurization performance of sulfided Ni–Mo catalysts: Effect of metal loading // China Pet. Process. Pe. 16(2) (2014) 12-19.

[44] E. Payen, R. Hubaut, S. Kasztelan, O. Poulet, J. Grimblot, Morphology Study of MoS_2- and WS_2-Based Hydrotreating Catalysts by High-Resolution Electron Microscopy // J. Catal. 147(1) (1994) 123-132.

[45] D. Ferdous, A. K. Dalai, J. Adjaye, L. Kotlyar, Surface morphology of NiMo/Al_2O_3 catalysts incorporated with boron and phosphorus: Experimental and simulation // Appl. Catal. A 294(1) (2005) 80–91.

[46] N. Frizi, P. Blanchard, E. Payen, P. Baranek, M. Rebeilleau, C. Dupuy, J. P. Dath, Genesis of new HDS catalysts through a careful control of the sulfidation of both Co and Mo atoms: Study of their activation under gas phase // Catal. Today 130 (2008) 272-282.

[47] M. Sun, P. J. Kooyman, R. Prins, A High-Resolution Transmission Electron Microscopy Study of the Influence of Fluorine on the Morphology and Dispersion of WS_2 in Sulfided W/Al_2O_3 and NiW/Al_2O_3 Catalysts // J. Catal. 206(2) (2002) 368–375.

[48] P. P. Minaev, P. A. Nikulshin, M. S. Kulikova, A. A. Pimerzin, V. M. Kogan, $NiWS/Al_2O_3$ hydrotreating catalysts prepared with 12-tungstophosphoric heteropolyacid and nickel citrate: Effect of Ni/W ratio // Appl. Catal. A 505 (2015) 456–466.

[49] D. Ishutenko, P. Minaev, Yu. Anashkin, M. Nikulshina, A. Mozhaev, K. Maslakov, P. Nikulshin, Potassium effect in $K\text{-}Ni(Co)PW/Al_2O_3$ catalysts for selective hydrotreating of model FCC gasoline // Appl. Catal. B 203 (2017) 237–246.

[50] A. Cordova, P. Blanchard, C. Lancelot, G. Frémy, C. Lamonier, Probing the Nature of the Active Phase of Molybdenum-Supported Catalysts for the Direct Synthesis of Methylmercaptan from Syngas and H_2S // ACS Catal. 5 (2015) 2966–2981.

[51] J. C. Mogica-Betancourt, A. Lopez-Benitez, J. R. Montiel-Lopez, L. Massin, M. Aouine, M. Vrinat, G. Berhault, A. Guevara-Lara, Interaction effects of nickel polyoxotungstate with the Al_2O_3–MgO support for application in dibenzothiophene hydrodesulfurization // J. Catal. 313 (2014) 9–23.

[52] K. B. Tayeb, C. Lamonier, C. Lancelot, M. Fournier, A. Bonduelle-Skrzypczak, F. Bertoncini, Increase of the Ni/W Ratio in Heteropolyanions Based NiW Hydrocracking Catalysts with Improved Catalytic Performances // Catal. Lett. 144 (2014) 460–468.

[53] L. Coulier, G. Kishan, J.A.R. van Veen, J. Niemantsverdriet, Influence of support-interaction on the sulfidation behavior and hydrodesulfurization activity of Al_2O_3-supported W, CoW, and NiW model catalysts // J. Phys. Chem. B 106 (2002) 5897–5906.

[54] M. Nikulshina, P. Blanchard, C. Lancelot, A. Griboval-Constant, M. Marinova, V. Briois, P. Nikulshin, C. Lamonier, Genesis of active phase in MoW/Al_2O_3 hydrotreating catalysts

monitored by HAADF and in situ QEXAFS combined to MCR-ALS analysis // Appl. Catal. B 269 (2020) 118766.

[55] S. Eijsbouts, L. C. A van den Oetelaar, R. R. van Puijenbroek, MoS_2 morphology and promoter segregation in commercial Type 2 Ni–Mo/Al_2O_3 and Co–Mo/Al_2O_3 hydroprocessing catalysts // J. Catal. 229 (2005) 352-364.

[56] Al. A. Pimerzin, P. A. Nikul'shin, A. V. Mozhaev, A. A. Pimerzin, Effect of surface modification of the support of hydrotreating catalysts with transition metal oxides (sulfides) on their catalytic properties // Petrol. Chem. 53(4) (2013) 245–254.

[57] M. Nikulshina, P. Blanchard, A. Mozhaev, C. Lancelot, A. Griboval-Constant, M. Fournier, C. Lamonier, Molecular approach to prepare mixed MoW alumina supported hydrotreatment catalysts using $H_4SiMo_nW_{12-n}O_{40}$ heteropolyacids // Catal. Sci. Technol. 8 (2018) 5557–5572.

[58] N. Koizumi, Y. Hamabe, S. Jung, Y. Suzuki, S. Yoshidaa and M. Yamada, In situ observation of Ni–Mo–S phase formed on NiMo/Al_2O_3 catalyst sulfided at high pressure by means of Ni and Mo K-edge EXAFS spectroscopy // J. Synchrotron Rad 17 (2010) 414–424.

[59] L. Plais, C. Lancelot, C. Lamonier, E. Payen, V. Briois, First in situ temperature quantification of CoMoS species upon gas sulfidation enabled by new insight on cobalt sulfide formation // Catal. Today (2020) https://doi.org/10.1016/j.cattod.2020.06.065.

[60] A. Rochet, B. Baubet, V. Moizan, E. Devers, A. Hugon, C. Pichon, E. Payen and V. Briois, Influence of the Preparation Conditions of Oxidic NiMo/Al_2O_3 Catalysts on the Sulfidation Ability: A Quick-XAS and Raman Spectroscopic Study // J. Phys. Chem. C 119 (2015) 23928–23942.

[61] H. Schulz, W. Bohringer, P. Waller, F. Ousmanov, Gas oil deep hydrodesulfurization: refractory compounds and retarded kinetics // Catal. Today 49 (1999) 87-97.

[62] V. La Vopa, C. N. Satterfield, Response of dienzothiophene hydrodesulfurization to presence of nitrogen compounds // Chem. Eng. Commun. 70 (1988) 171–176.

[63] R. Prins, Catalytic hydrodenitrogenation // Adv. Catal. 46 (2001) 399–464.

[64] M. Egorova, R. Prins, Competitive hydrodesulfurization of 4,6-dimethyldibenzothiophene, hydrodenitrogenation of 2-methylpyridine, and hydrogenation of naphthalene over sulfided NiMo/γ-Al_2O_3 // J. Catal. 224 (2004) 278-287.

[65] G. C. Laredo, A. Montesinos, J. A. De los Reyes, Inhibition effects observed between dibenzothiophene and carbazole during the hydrotreating process // Appl. Catal. A 265 (2004) 171-183.

[66] A. Stanislaus, A. Marafi, M. S. Rana, Recent advances in the science and technology of ultra low sulfur diesel (ULSD) production // Catal. Today 153 (2010) 1-68.

[67] H. Topsøe, B. S. Clausen, F. E. Massoth, in: J. R. Anderson, M. Boudart (Eds.), Hydrotreating Catalysis, Springer-Verlag, Berlin–Heidelberg–N.Y., 1996, p. 310.

[68] E. Schachtl, E. Kondratieva, O. Y. Gutiérrez, J. A. Lercher, Pathways for H_2 Activation on (Ni)-MoS_2 Catalysts // J. Phys. Chem. Lett. 6 (2015) 2929–2932.

[69] S. Albersberger, H. Shi, M. Wagenhofer, J. Han, O. Y. Gutiérrez, J. A. Lercher, On the enhanced catalytic activity of acid-treated, trimetallic Ni-Mo-W sulfides for quinoline hydrodenitrogenation // J. Catal. 380 (2019) 332–342.

[70] A. Olivas, D. H. Galván, G. Alonso, S. Fuentes, Trimetallic NiMoW unsupported catalysts for HDS // Appl. Catal. A 352 (2009) 10–16.

[71] C. Yin, H. Liu, L. Zhao, B. Liu, S. Xue, N. Shen, Y. Liu, Y. Li, C. Liu, Study for the production of ultra-low sulfur gas oils on a highly loaded NiMoW catalyst // Catal. Today 259 (2016) 409–416.

[72] M. S. Nikul'shina, A. V. Mozhaev, C. Lancelot, P. Blanchard, C. Lamonier, P. A. Nikul'shin, Effect of Quinoline on Hydrodesulfurization and Hydrogenation on Bi- and Trimetallic NiMo(W)/Al_2O_3 Hydrotreating Catalysts // Russ. J. Appl. Chem. 92 (1) (2019) 105-112.

[73] N. N. Tomina, P. C. Solmanov, N. M. Maksimov, A. A. Pimerzin, Hydrotreatment of petroluem on Ni_6-$PMo_nW_{(12-n)}(S)/Al_2O_3$ catalysts // Catal. Ind. 7 (4) (2015) 307-313.

[74] S. L. González-Cortés, S. Rugmini, T. Xiao. M. L. H. Green, S. M. Rodulfo-Baechler, F. E. Imbert, Deep hydrotreating of different feedstocks over a highly active Al_2O_3-supported NiMoW sulfide catalyst // Appl. Catal. A 475 (2014) 270–281.

[75] M. Absi-Halabi, A. Stanislaus, K. Al-Dolama, Performance comparison of alumina-supported Ni-Mo, Ni-W and Ni-Mo-W catalysis in hydrotreating vacuum residue // Fuel 77 (7) (1998) 787-790.

[76] A. Griboval, P. Blanchard, E. Payen, M. Fournier, J.L. Dubois, J.R. Bernard, Characterization and catalytic performances of hydrotreatment catalysts prepared with silicium heteropolymolybdates: comparison with phosphorus doped catalysts // Appl. Catal. A 217 (2001) 173–183.

[77] L. Lizama, T. Klimova, Highly active deep HDS catalysts prepared using Mo and W heteropolyacids supported on SBA-15 // Appl. Catal. B 82 (2008) 139–150.

[78] S. Shan, H. Liu, G. Shi, X. Bao, Tuning of the active phase structure and hydrofining performance of alumina-supported tri-metallic WMoNi catalysts via phosphorus incorporation // Front. Chem. Sci. Eng. 12(1) (2018) 59-69.

1

2

3

Captions for Tables

Table 1. Composition and textural characteristics of sulfided NiMo(W)/Al_2O_3 catalysts.

Table 2. Catalytic properties of NiMo(W)/Al_2O_3 catalysts in HDT of a mixture of DBT and naphthalene.

Table 3. Catalytic properties of NiMo(W)/Al_2O_3 catalysts in HDT of a mixture of DBT, naphthalene and quinoline.

Table 4. Composition of hydrogenation products obtained in the process of SRGO hydrotreating over the synthesized NiMo(W)/Al_2O_3 catalysts.

Table 5. Morphological characteristics of the NiMo(W)S active phase species calculated from TEM micrographs.

Table 6. Relative metal fractions measured by XPS for Ni, Mo and W species present at the surface of sulfided NiMo(W)/Al_2O_3 catalysts.

Table 7. Structural parameters obtained by multi-edge fitting from the Fourier-analysis of Mo *K*- and W L_3-edges EXAFS spectra of sulfided NiMo(W)/Al_2O_3 catalysts.

Table 8. Synergistic effects of structure-formed metals (Mo and W) in bulk and supported (Ni)MoW catalysts.

Captions for Figures

Figure 1. Dependence of reaction rate constants in DBT HDS (a), naphthalene HYD (b) and selectivity route of DBT HDS (c) on Mo/(Mo+W) atomic ratio in NiMo(W)/Al_2O_3 catalysts (circles correspond to $NiMo_nW_{12-n}/Al_2O_3$ catalysts; squares are $Ni(Mo_n+W_{12-n})/Al_2O_3$ catalysts; dotted line indicates additive values between $NiMo_{12}/Al_2O_3$ and NiW_{12}/Al_2O_3).

Figure 2. Dependence of reaction rate constants in DBT HDS (a), naphthalene HYD (b), quinoline HDN (c) and selectivity route of DBT HDS (d) on Mo/(Mo+W) atomic ratio in NiMo(W)/Al_2O_3 catalysts (circles correspond to $NiMo_nW_{12-n}/Al_2O_3$ catalysts; squares are $Ni(Mo_n+W_{12-n})/Al_2O_3$ catalysts; dotted line indicates additive values between $NiMo_{12}/Al_2O_3$ and NiW_{12}/Al_2O_3).

Figure 3. Inhibition effect on the HDS of DBT (a) and naphthalene HYD (b) in the presence of quinoline.

Figure 4. TOF_{edge} number in DBT HDS (a), HYD naphthalene (b) and HDN quinoline (c) over NiMo(W)/Al_2O_3 catalysts in the presence of quinoline.

Figure 5. Dependence of reaction rate constants k_{HDS} (a), HYD (b) and HDN (c) activities in HDT of SRGO on Mo/(Mo+W) atomic ratio in NiMo(W)/Al_2O_3 catalysts (dotted line indicates additive values between $NiMo_{12}/Al_2O_3$ and NiW_{12}/Al_2O_3).

Figure 6. HAADF images of sulfided $NiMo_3W_9/Al_2O_3$ (a) and $Ni(Mo_3+W_9)/Al_2O_3$ (c) catalysts with intensity profile corresponding to the row of atoms identified by the arrow on $NiMo_3W_9/Al_2O_3$ (b).

Figure 7. k^3-weighted EXAFS at the Mo *K*-edge and W L_3-edge, and the corresponding Fourier transforms of sulfided NiMo(W)/Al_2O_3 catalysts.

Figure 8. Ni *K*-edge XANES spectra comparison (A): (a) Ni/Al_2O_3 and bimetallic samples, (b) Ni/Al_2O_3 and trimetallic samples, (c) $NiMo_{12}$/Al_2O_3 and trimetallic samples, (d) Ni(Mo_3+W_9)/Al_2O_3 and bimetallic catalysts; Comparison of k^3-weighted EXAFS spectra of sulfided catalysts (B): (a) Ni/Al_2O_3 and bimetallic samples, (b) Ni/Al_2O_3 and trimetallic catalysts.

Figure 9. 3D dependence of the TOF_{edge} number in DBT HDS reaction (co-hydrotreating of DBT, naphthalene and quinoline) on the Ni/$(Mo+W)_{edge}$ promotion degree and Mo/(Mo+W) atomic ratio.

1

Table 1. Composition and textural characteristics of sulfided NiMo(W)/Al_2O_3 catalysts.

Catalyst	Content (wt. %)			Textural characteristics		
	Mo	W	Ni	S_{BET} (m^2 g^{-1})	V_p (cm^3 g^{-1})	D (nm) [a]
NiW_{12}	-	20.8	3.3	240	0.58	3.8/8.4
$NiMo_1W_{11}$	0.9	19.0	3.4	202	0.47	3.8/8.4
$NiMo_3W_9$	2.8	15.9	3.4	233	0.49	3.8/8.4
$NiMo_6W_6$	5.5	10.5	3.4	205	0.48	3.8/8.2
$NiMo_9W_3$	8.4	8.7	3.5	225	0.48	3.8/8.4
$Ni(Mo_1+W_{11})$	0.9	19.0	3.4	230	0.51	3.8/8.4
$Ni(Mo_3+W_9)$	2.8	15.9	3.4	210	0.48	3.8/8.4
$Ni(Mo_6+W_6)$	5.5	10.5	3.4	216	0.50	3.8/8.4
$Ni(Mo_9+W_3)$	8.4	8.7	3.5	233	0.53	3.7/8.6
$NiMo_{12}$	12.0	-	3.7	236	0.42	3.8/8.4

[a] bimodal pore size distribution.

Table 2. Catalytic properties of NiMo(W)/Al_2O_3 catalysts in HDT of a mixture of DBT and naphthalene.

Catalysts	Conversion (%)		$k\times10^4$ (mol h^{-1} g^{-1})		$TOF_{edge}\times10^3$ (s^{-1})		$S_{HYD/DDS}$
	DBT HDS	Naphthalene HYD	k_{HDS}	k_{HYD}	HDS	HYD	
NiW_{12} [a]	49.0 ± 1.5	39.6 ± 0.6	16.4 ± 0.7	60.2 ± 2.3	3.64 ± 0.11	14.5 ± 0.4	0.32 ± 0.01
$NiMo_1W_{11}$ [a]	60.1 ± 1.8	36.8 ± 1.1	22.3± 1.1	56.3 ± 2.1	3.93 ± 0.12	12.1 ± 0.4	0.34 ± 0.02
$NiMo_3W_9$ [a]	73.2 ± 2.2	38.9 ± 1.2	31.9 ± 2.0	60.2 ± 2.7	4.25 ± 0.13	11.4 ± 0.3	0.19 ± 0.01
$NiMo_6W_6$	71.6	37.3	30.6	56.8	3.39	8.8	0.21
$NiMo_9W_3$	75.4	38.9	34.2	60.0	3.04	7.9	0.24
$Ni(Mo_1+W_{11})$ [a]	49.0 ± 1.0	35.0 ± 0.7	16.4 ± 0.5	52.5 ± 1.3	3.44 ± 0.09	12.6 ± 0.3	0.49 ± 0.03
$Ni(Mo_3+W_9)$	42.0	32.1	13.3	47.0	2.99	11.4	0.36
$Ni(Mo_6+W_6)$	60.4	33.0	22.5	48.8	3.50	9.6	0.24
$Ni(Mo_9+W_3)$	72.7	37.6	31.6	58.9	3.41	8.8	0.20
$NiMo_{12}$ [a]	70.8 ± 2.1	49.2 ± 1.4	29.9 ± 1.8	79.2 ± 3.3	3.47 ± 0.10	11.7 ± 0.4	0.13 ± 0.01

(Test conditions: T=280°C, LHSV= 40 h^{-1}, K_H=500 NL L^{-1}, P = 3.0 MPa)

[a] samples have been tested twice

Table 3. Catalytic properties of NiMo(W)/Al_2O_3 catalysts in HDT of a mixture of DBT, naphthalene and quinoline.

Catalysts	Conversion (%)			$k\times10^4$ (mol·g^{-1}·h^{-1})			$TOF_{edge}\times10^3$ (s^{-1})			$S_{HYD/DDS}$
	DBT HDS	Naphthalene HYD	Quinoline HDN [b]	HDS	HYD	HDN	HDS	HYD	HDN	
NiW_{12} [a]	65.0 ± 2.0	11.0 ± 0.3	10.2 ± 0.4	25.5 ± 1.4	14.2 ± 0.5	2.0 ± 0.1	4.8 ± 0.2	4.1 ± 0.1	0.58 ± 0.02	0.24 ± 0.02
$NiMo_1W_{11}$ [a]	77.9 ± 2.3	14.2 ± 0.4	21.2 ± 0.6	36.8 ± 2.7	18.6 ± 0.6	4.4 ± 0.1	5.1 ± 0.2	4.7 ± 0.2	1.06 ± 0.03	0.03 ± 0.00
$NiMo_3W_9$ [a]	72.0 ± 2.2	7.2 ± 0.3	19.4 ± 0.7	31.0 ± 1.9	9.1 ± 0.4	4.0 ±0.1	4.2 ± 0.1	2.1 ±0.1	0.86 ± 0.03	0.02 ± 0.00
$NiMo_6W_6$	70.2	6.4	17.0	29.5	8.0	3.4	3.3	1.5	0.61	0.01
$NiMo_9W_3$	73.2	6.0	14.3	32.0	7.5	2.9	3.0	1.2	0.44	0.01
$Ni(Mo_1+W_{11})$ [a]	70.0 ± 1.4	6.9 ± 0.3	15.0 ± 0.5	29.3 ± 1.1	8.8 ± 0.4	3.0 ± 0.1	5.0 ± 0.1	2.5 ± 0.1	0.82 ± 0.03	0.08± 0.01
$Ni(Mo_3+W_9)$	60.0	4.0	14.5	22.3	5.0	2.9	4.3	1.5	0.79	0.05
$Ni(Mo_6+W_6)$	68.0	4.8	13.8	27.8	6.0	2.7	3.9	1.4	0.61	0.01
$Ni(Mo_9+W_3)$	71.3	5.4	13.2	30.3	6.7	2.6	3.4	1.3	0.47	0.01
$NiMo_{12}$ [a]	79.6 ± 2.4	6.4 ± 0.3	11.8 ± 0.4	38.8 ± 2.9	8.0 ± 0.3	2.3 ± 0.1	3.9 ±0.1	1.6 ±0.1	0.44 ± 0.02	0.09 ± 0.01

(Test conditions: T=280℃, LHSV= 40 h^{-1}, K_H=500 NL L^{-1}, P = 3.0 MPa)

[a] samples tested twice;

[b] indicates the depth of nitrogen removal (%).

Table 4. Composition of hydrogenation products obtained in the process of SRGO hydrotreating over the synthesized NiMo(W)/Al_2O_3 catalysts.

Catalyst	Content in hydrogenation product					Rate constants k_{HDS} (h^{-1} (wt. % S)$^{-0.4}$)
	S (ppm)	N (ppm)	Aromatics (wt. %)			
			mono-	bi-	tri-	
Feedstock	8147	156	31.9	10.03	2.46	-
NiW_{12} [a]	114.1 ± 5.1	42.1 ± 2.6	31.8 ± 0.8	4.02 ± 0.08	0.84 ± 0.02	29.1 ± 0.7
$NiMo_1W_{11}$ [a]	48.8 ± 3.0	22.7 ± 1.6	30.7 ± 0.8	3.54 ± 0.07	0.66 ± 0.01	44.8 ± 1.3
$NiMo_3W_9$ [a]	40.9 ± 1.9	14.0 ± 0.9	30.9± 0.6	3.35 ± 0.05	0.66 ± 0.01	49.2 ± 1.2
$NiMo_6W_6$	45.3	17.0	29.8	3.39	0.63	47.1
$NiMo_9W_3$	52.2	22.2	31.7	3.40	0.70	43.8
$Ni(Mo_1+W_{11})$ [a]	74.5 ± 3.1	30.2 ± 1.1	30.9 ± 0.7	3.66 ± 0.04	0.80 ± 0.02	35.6 ± 0.7
$Ni(Mo_3+W_9)$ [a]	46.6 ± 2.6	20.0 ± 1.1	30.4 ± 0.6	3.71 ± 0.06	0.79 ± 0.02	45.9 ± 1.2
$Ni(Mo_6+W_6)$	50.1	20.9	31.4	3.40	0.77	44.6
$Ni(Mo_9+W_3)$	58.7	30.3	31.7	3.70	0.74	41.0
$NiMo_{12}$	73.8	25.4	30.6	3.44	0.80	36.5

[a] samples have been tested twice

Table 5. Morphological characteristics of the NiMo(W)S active phase species calculated from TEM micrographs.

Catalyst	Average length $\bar{L}$ (nm)	Average stacking number $\bar{N}$	Dispersion of NiMo(W)S particles D	Distribution of slab length (rel. %)				Distribution of stacking number (rel. %)			
				<2	2..4	4..6	>6	1	2	3	>3
NiW_{12}	3.9	2.1	0.30	3	52	40	5	30	38	27	5
$NiMo_1W_{11}$	3.8	2.1	0.31	7	38	48	7	32	29	29	9
$NiMo_3W_9$	3.6	1.8	0.32	6	61	30	3	36	49	12	3
$NiMo_6W_6$	3.7	2.0	0.32	2	64	29	5	31	43	22	4
$NiMo_9W_3$	3.6	1.9	0.32	12	55	29	4	34	49	13	3
$Ni(Mo_1+W_{11})$	3.7	1.9	0.32	3	60	31	6	40	42	11	8
$Ni(Mo_3+W_9)$	3.6	1.4	0.32	1	67	28	4	58	39	3	0
$Ni(Mo_6+W_6)$	4.1	1.9	0.29	1	49	40	10	31	45	18	6
$Ni(Mo_9+W_3)$	3.8	1.7	0.31	0	64	29	7	44	44	11	0
$NiMo_{12}$	3.4	1.6	0.34	2	73	25	0	42	52	6	0

Table 6. Relative metal fractions measured by XPS for Mo, W and Ni species present at the surface of sulfided NiMo(W)/Al_2O_3 catalysts.

Catalyst	Ni percentage (rel. %)			Mo percentage (rel. %)			W percentage (rel. %)			$Ni(Mo+W)_{edge}$
	NiMo(W)S	NiS	Ni^{2+}	MoS_2	MoS_xO_y	Mo^{6+}	WS_2	WS_xO_y	W^{6+}	
NiW_{12}	30	56	14	-	-	-	64	7	29	0.74
$NiMo_1W_{11}$	37	51	12	72	28	0	69	10	21	0.82
$NiMo_3W_9$	42	54	4	74	26	0	74	8	18	0.82
$NiMo_6W_6$	40	50	10	71	26	4	73	7	20	0.88
$NiMo_9W_3$	43	49	8	69	25	6	77	8	15	0.92
$Ni(Mo_1+W_{11})$	35	55	10	70	30	0	59	9	33	0.79
$Ni(Mo_3+W_9)$	36	43	21	67	19	14	59	7	34	0.87
$Ni(Mo_6+W_6)$	37	44	19	63	22	15	61	10	29	0.97
$Ni(Mo_9+W_3)$	39	43	18	60	23	17	64	9	27	0.99
$NiMo_{12}$	62	27	11	73	15	12	-	-	-	0.90

Table 7. Structural parameters obtained by multi-edge fitting from the Fourier-analysis of Mo *K*- and W L_3-edges EXAFS spectra of sulfided NiMo(W)/Al_2O_3 catalysts.

Scattering path	*N*	*R* (Å)	σ^2 x 10^3 (Å²)	E_0 (eV)	*R*-factor
$NiMo_{12}/Al_2O_3$					
Mo-S	5.4 ± 0.5	2.41 ± 0.01	3.2 ± 0.7	1.9 ± 0.8	0.0057
Mo-Mo	3.7 ± 0.7	3.18 ± 0.01	4.0 ± 0.9		
NiW_{12}/Al_2O_3					
W-S	5.8 ± 0.7	2.41 ± 0.01	3.0 ± 0.9	7.7 ± 1.6	0.0105
W-W	4.3 ± 1.1	3.16 ± 0.01	4.3 ± 1.0		
$NiMo_3W_9/Al_2O_3$					
Mo-S	5.5 ± 0.5	2.42±0.01	3.3 ± 0.8		
Mo-Mo	1.5 ± 0.6	3.21±0.02	4.8 ± 2.3	3.0±1.0	
Mo-W	2.8 ± 1.2	3.20±0.01	4.8 ± 2.3		0.010
W-S	6.1 ± 0.7	2.41±0.01	3.0± 0.8		
W-W	2.8 ± 1.6	3.17±0.01	4.8 ± 2.3	9.0 ±1.7	
$Ni(Mo_3+W_9)/Al_2O_3$					
Mo-S	5.9 ± 0.9	2.42 ± 0.01	3.4 ± 1.0		
Mo-Mo	3.3 ± 0.8	3.19 ± 0.01	4.4 ± 1.1	2.9 ± 2.0	
Mo-W	1.6 ± 0.8	3.19 ± 0.03	4.4 ± 1.1		0.0058
W-S	5.6 ± 0.4	2.41 ± 0.01	2.9 ± 0.5		
W-W	3.5 ± 0.8	3.17 ± 0.01	4.4 ± 1.1	9.2 ± 1.3	

Table 8. Synergistic effects of structure-formed metals (Mo and W) in bulk and supported (Ni)MoW catalysts.

Catalyst	Mo/W ratio investigated	Reaction	Mo/W ratio with highest activity	Synergistic effect of Mo and W	Possible reason	Reference
NiMoW/Al_2O_3	0.1, 0.3, 1, 3	HDS of DBT, HYD of Naphthalene HDN of Quinoline HDT of SRGO	0.3-3 0.3-3 0.1-0.3 0.3	Discovered	More amount of mixed $MoWS_2$ particles. Hydrogenation ability depends on Mo/W ratio and feeds	Present work
MoW/Al_2O_3	0.1, 0.3, 1, 3	HDS of DBT, HYD of Naphthalene	1	Discovered	More amount of mixed $MoWS_2$ particles with core-shell structure	[13]
NiMoW/Al_2O_3	0.3, 1.0, 3	HDS of DBT HDT of SRGO	- 3	No Discovered	Trimetallic catalysts may have enhanced HYD activity, while the hydrogenolysis activity is unaffected	[11]
NiMoW bulk	0.5, 1, 2	HDN of quinoline	0.5-2	Discovered	Trimetallic active phase has high concentration of sulfur vacancies (SH groups)	[69]

NiMoW/MWCNT	2.6, 3.8, 8	HDS thiophene	3.8	Discovered	Positive effect of metal-support interaction, dispersion of active phase species	[12]
NiMoW bulk	0.75, 0.85, 0.95	HDS of DBT	0.85	Discovered	Increasing metallic character of mixed $MoWS_2$ phase (DFT calculations)	[70]
NiMoW/Al_2O_3	1	HDS of thiophene HDT of SRGO	1	Discovered	The E_{MS} value of NiMoWS phase was improved, becoming closer to the volcano curve's optimum and a new synergy effect with respect to NiMoS and NiWS phases was subsequently expected.	[22]
NiMoW/Al_2O_3	0.5, 1.0, 2.0	HDS of DBT HDT of mixture oil	1	Discovered	Enhancing sulfur mobility (not confirmed)	[73]
NiMoW bulk	1.0	HDT of FCC gas oil, coking gas oil	1	Discovered	The results are explained in terms of higher hydrogenation activity owing to the incorporation of W	[71]

$NiMoW/Al_2O_3$	1.4	HDT of vacuum residue feedstock	1.4	Discovered	The results are explained in terms of higher hydrogenation activity owing to the incorporation of W	[75]
NiMoW/Al-HMS	1	HDS of DBT	1	Discovered	The results are explained in terms of higher hydrogenation activity owing to the incorporation of W	[23]
$NiMoW/Al_2O_3$	1.0	HDS of DBT HDT of FCC diesel	1	Discovered	Increased degree of metal sulfidation and amount of active phase	[5]

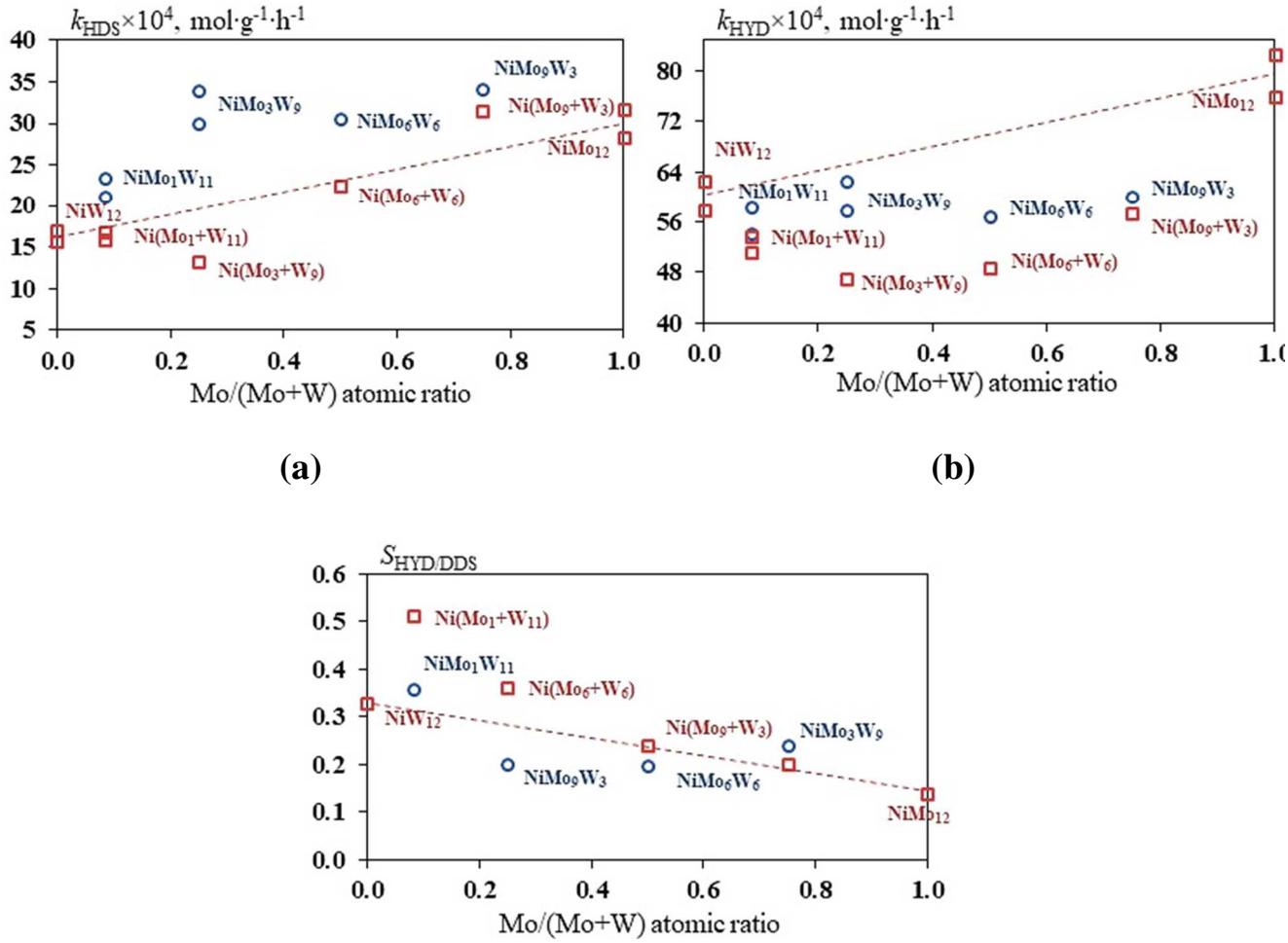

Fig. 1. Dependence of reaction rate constants in DBT HDS (a), naphthalene HYD (b) and selectivity route of DBT HDS (c) on Mo/(Mo+W) atomic ratio in NiMo(W)/Al_2O_3 catalysts (circles correspond to $NiMo_nW_{12-n}/Al_2O_3$ catalysts; squares are $Ni(Mo_n+W_{12-n})/Al_2O_3$ catalysts; dotted line indicates additive values between $NiMo_{12}/Al_2O_3$ and NiW_{12}/Al_2O_3).

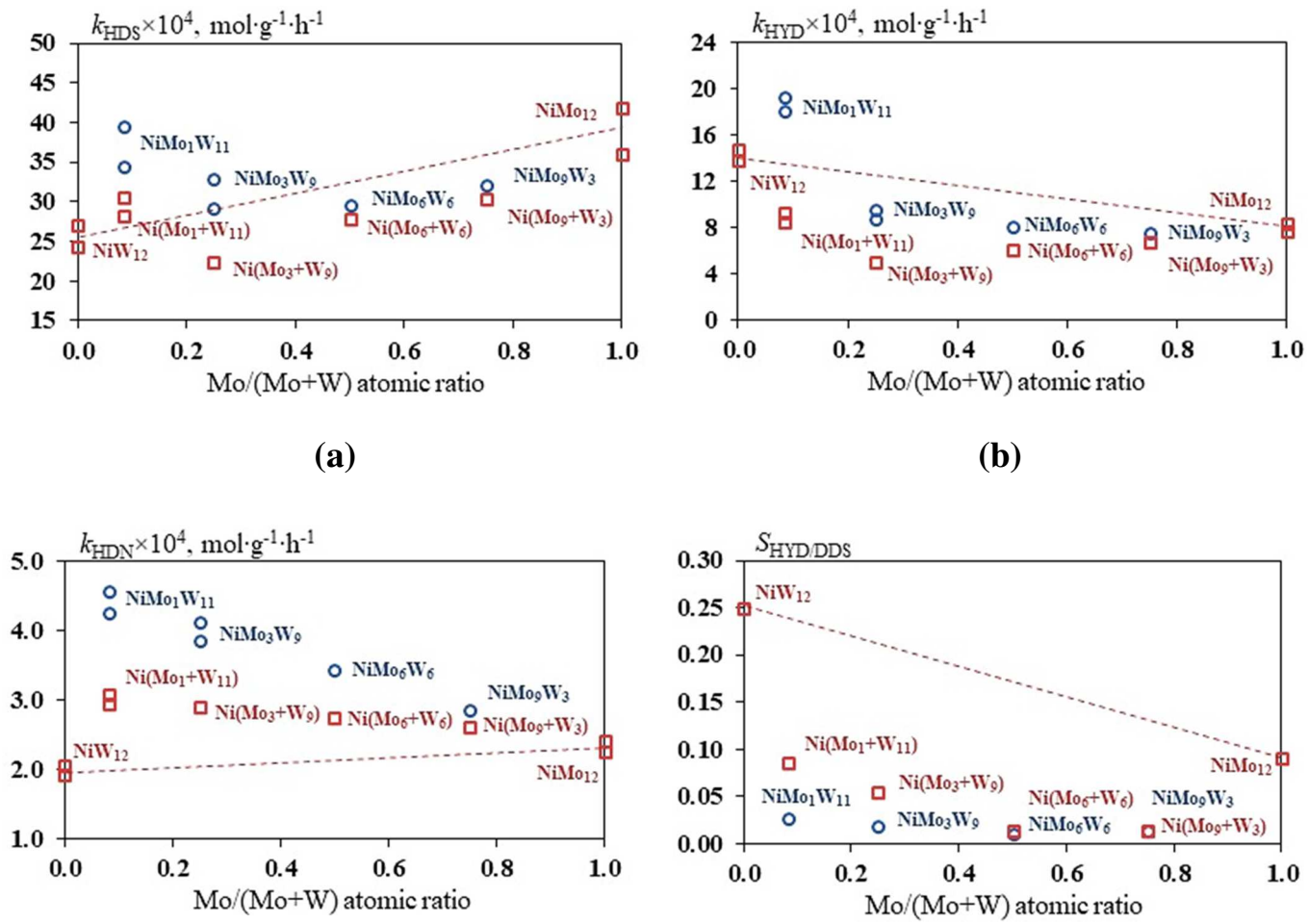

Fig. 2. Dependence of reaction rate constants in DBT HDS (a) naphthalene HYD (b), quinoline HDN (c) and selectivity route of DBT HDS (d) on Mo/(Mo+W) atomic ratio in NiMo(W)/Al_2O_3 catalysts (circles correspond to $NiMo_nW_{12-n}/Al_2O_3$ catalysts; squares are $Ni(Mo_n+W_{12-n})/Al_2O_3$ catalysts; dotted line indicates additive values between $NiMo_{12}/Al_2O_3$ and NiW_{12}/Al_2O_3).

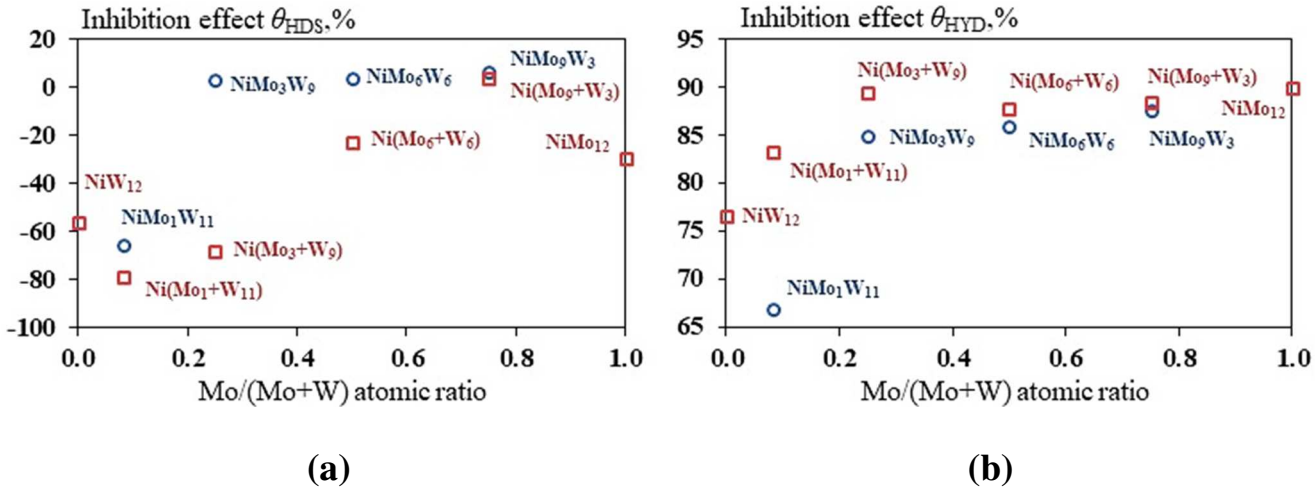

(a) **(b)**

Fig. 3. Inhibition effect in the HDS of DBT (a) and naphthalene HYD (b) in presence of quinoline.

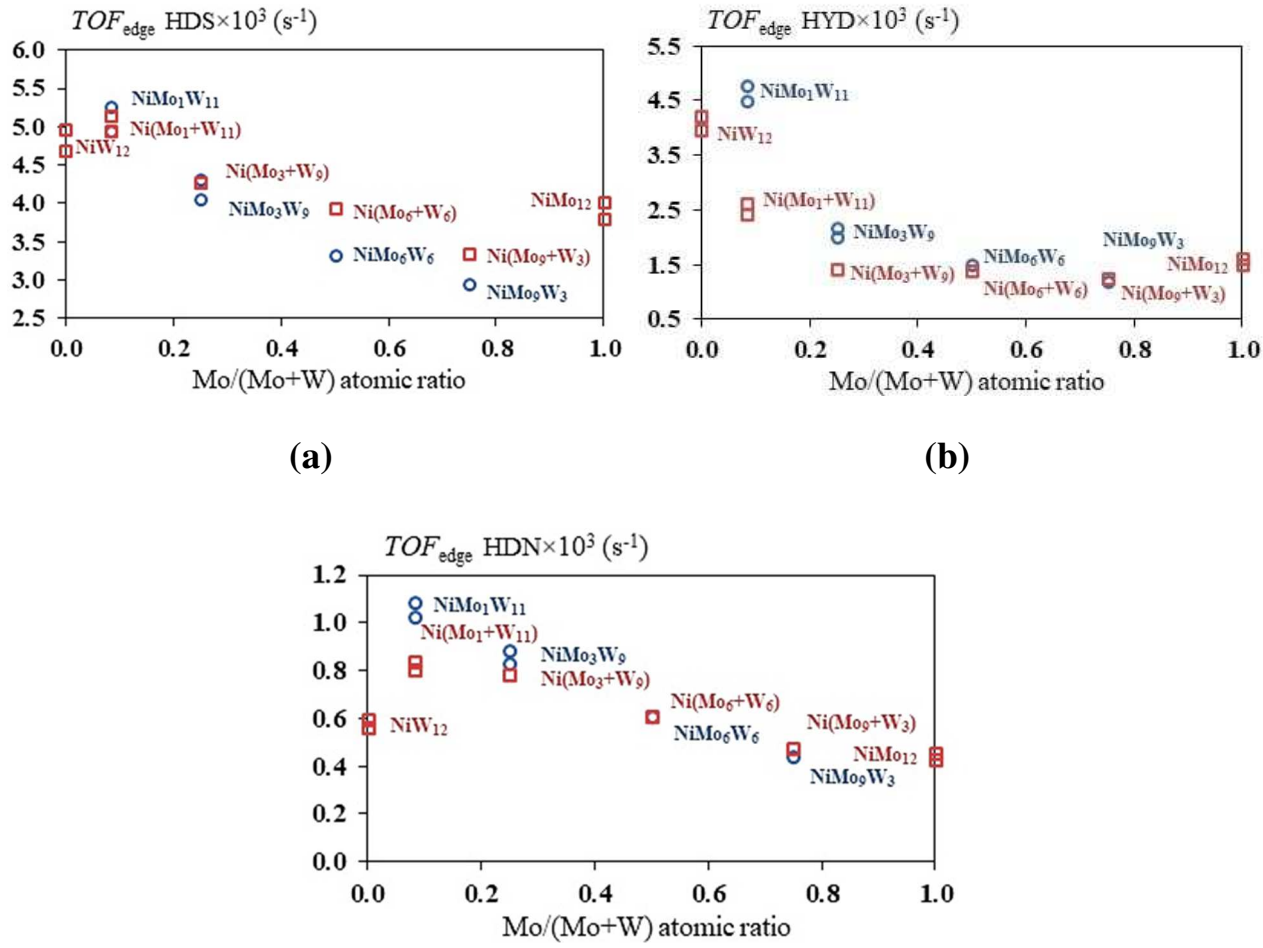

Fig. 4. TOF_{edge} number in DBT HDS (a), HYD naphthalene (b) and HDN quinoline (c) over NiMo(W)/Al_2O_3 catalysts in the presence of quinoline.

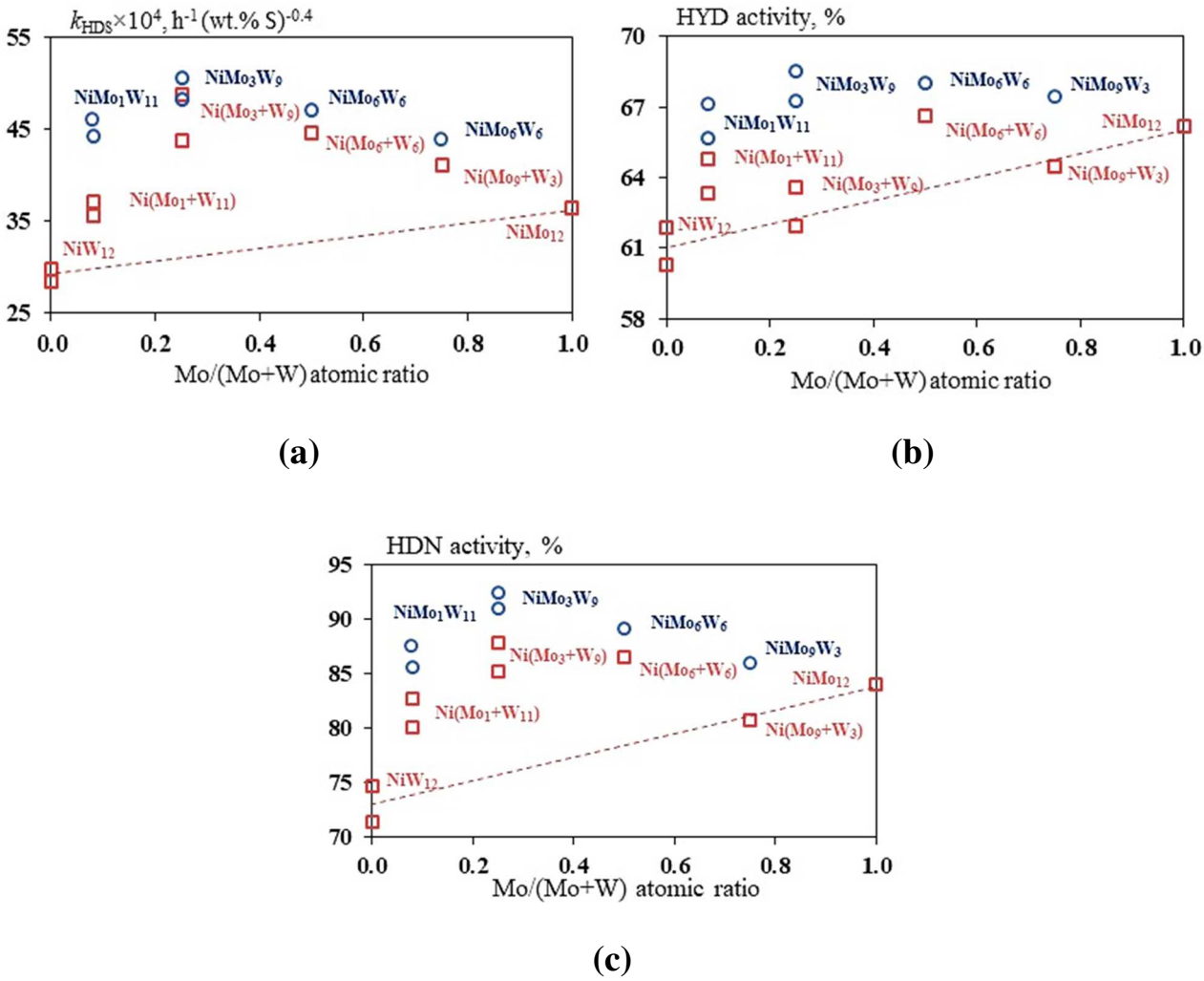

Fig. 5. Dependence of reaction rate constants k_{HDS} (a), HYD (b) and HDN (c) activities in HDT of SRGO on Mo/(Mo+W) atomic ratio in NiMo(W)/Al_2O_3 catalysts (dotted line indicates additive values between $NiMo_{12}/Al_2O_3$ and NiW_{12}/Al_2O_3).

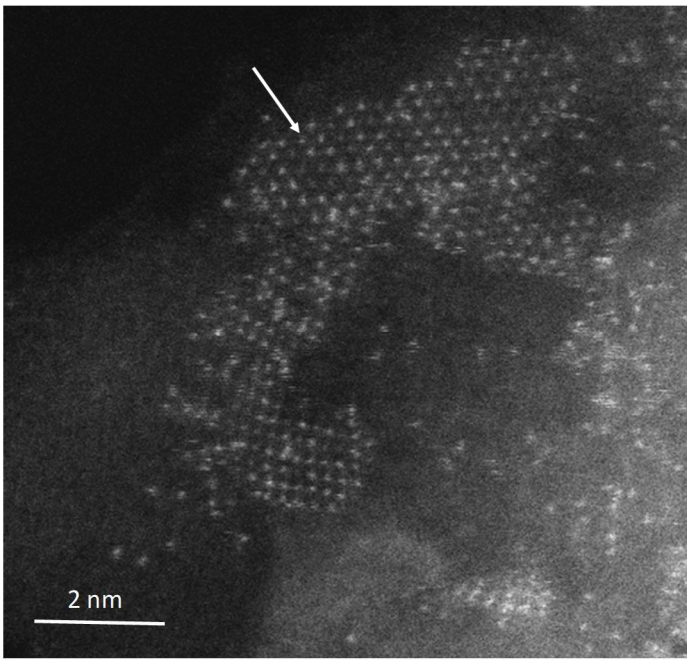

(a)

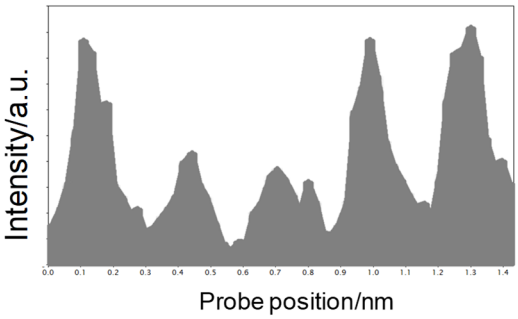

(b)

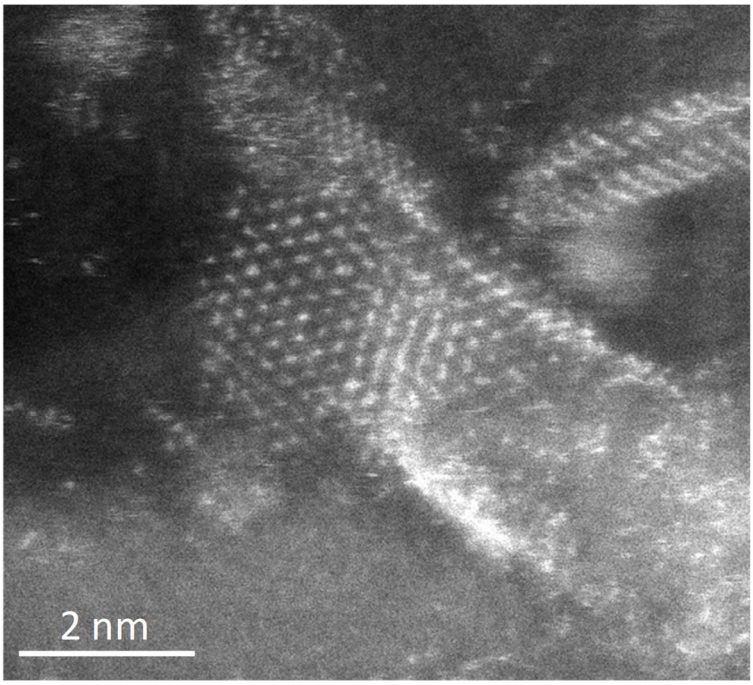

(c)

Fig. 6. HAADF images of sulfided $NiMo_3W_9/Al_2O_3$ (a) and $Ni(Mo_3+W_9)/Al_2O_3$ (c) catalysts with intensity profile corresponding to the row of atoms identified by the arrow on $NiMo_3W_9/Al_2O_3$ (b).

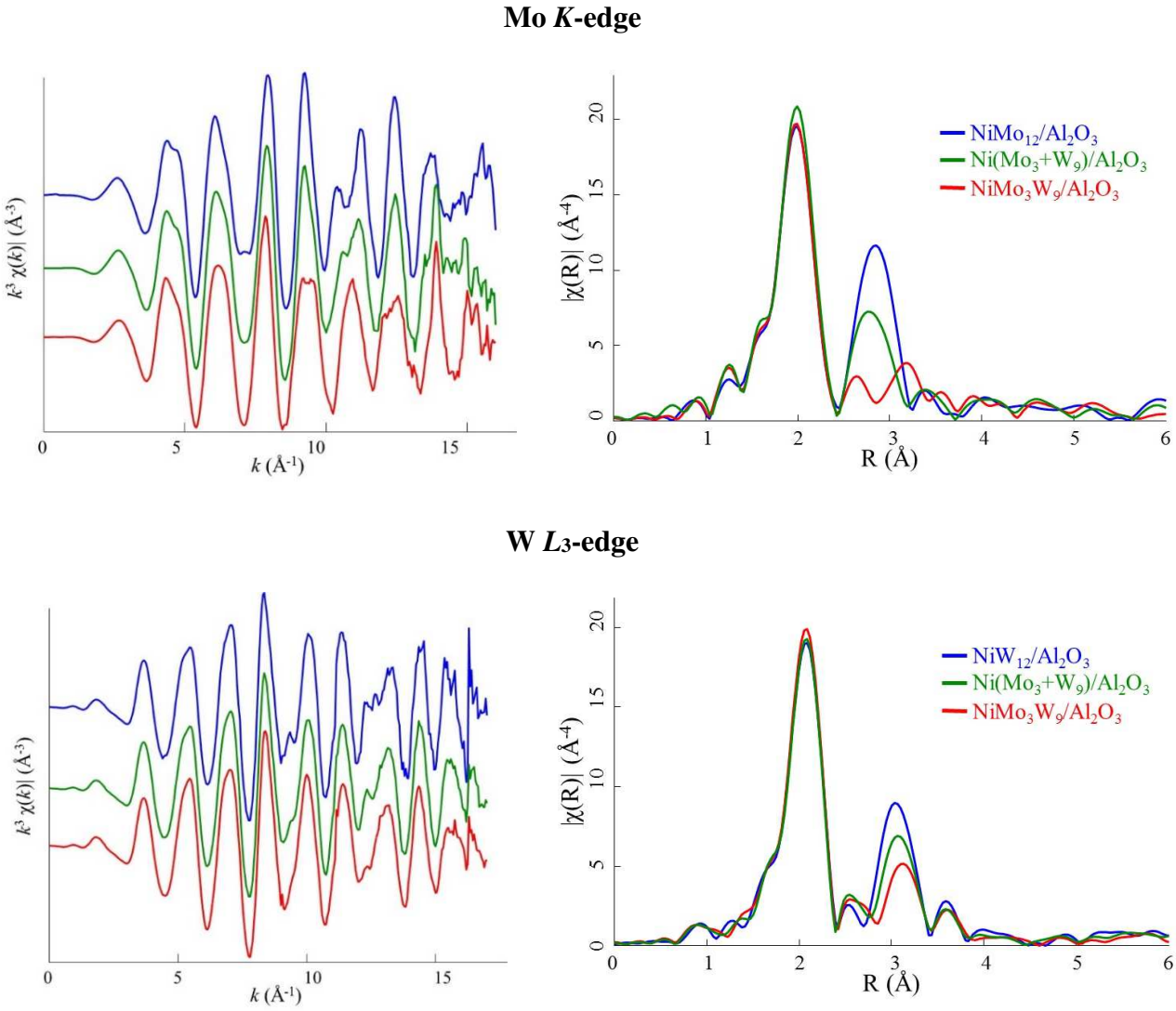

Fig. 7. k^3-weighted EXAFS at the Mo *K*-edge and W L_3-edge, and the corresponding Fourier transforms of sulfided NiMo(W)/Al_2O_3 catalysts.

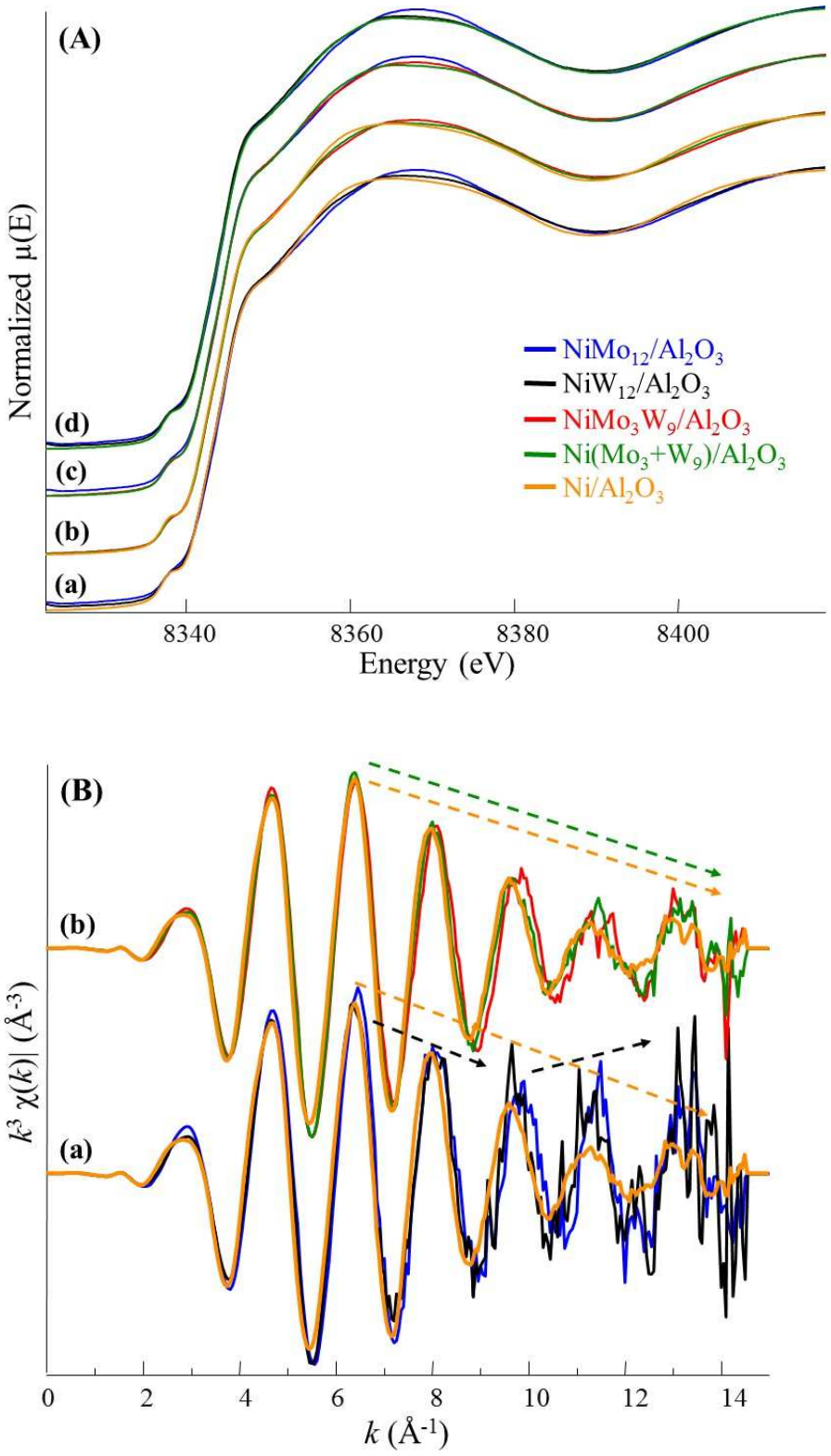

Fig. 8. Ni *K*-edge XANES spectra comparison (A): (a) Ni/Al_2O_3 and bimetallic samples, (b) Ni/Al_2O_3 and trimetallic samples, (c) $NiMo_{12}/Al_2O_3$ and trimetallic samples, (d) $Ni(Mo_3+W_9)/Al_2O_3$ and bimetallic catalysts; Comparison of k^3-weighted EXAFS spectra of sulfided catalysts (B): (a) Ni/Al_2O_3 and bimetallic samples, (b) Ni/Al_2O_3 and trimetallic catalysts.

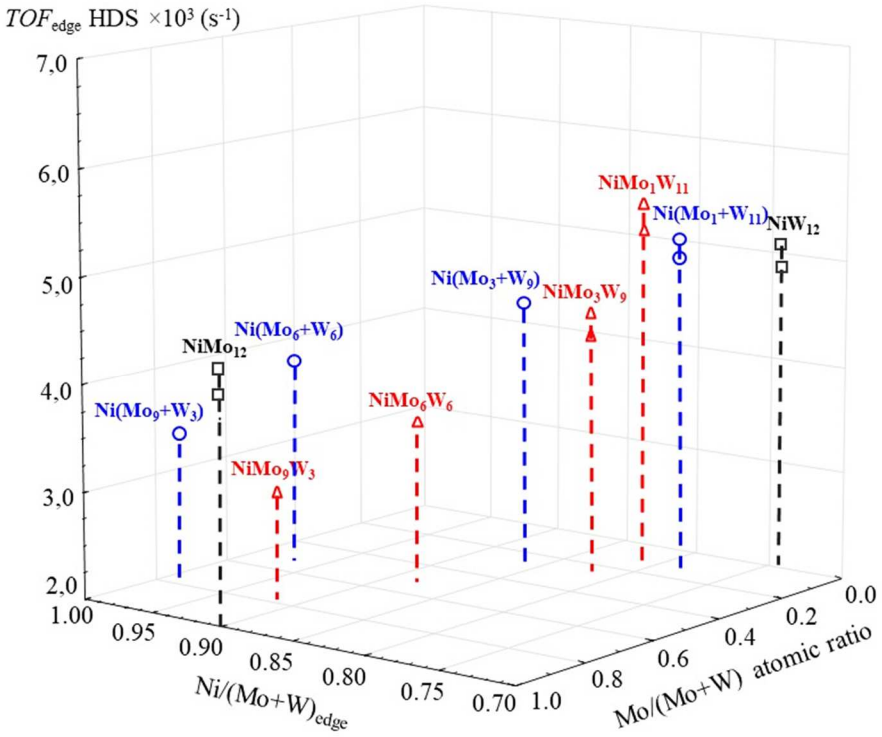

Fig. 9. 3D dependence of the TOF_{edge} number in DBT HDS reaction (co-hydrotreating of DBT, naphthalene and quinoline) on the $Ni/(Mo+W)_{edge}$ promotion degree and Mo/(Mo+W) atomic ratio.